UNIVERSITY OF THESSALY
SCHOOL OF ENGINEERING
DEPARTMENT OF MECHANICAL ENGINEERING
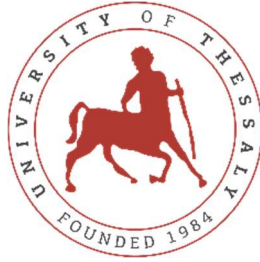
FLOW INDUCED VIBRATIONS IN PIPING

by

Lydia Lymperopoulou

Supervisor
Prof. Spyros A. Karamanos

Submitted in partial fulfillment of the requirements for the degree of Diploma in
Mechanical Engineering at the University of Thessaly

Volos, 2022

UNIVERSITY OF THESSALY
SCHOOL OF ENGINEERING
DEPARTMENT OF MECHANICAL ENGINEERING

FLOW INDUCED VIBRATIONS IN PIPING

by

Lydia Lymperopoulou

Supervisor
Prof. Spyros A. Karamanos

Submitted in partial fulfillment of the requirements for the degree of Diploma in
Mechanical Engineering at the University of Thessaly

Volos, 2022

Approved by the Committee on Final Examination:

Advisor: Dr. Spyros A. Karamanos,
        Professor, Department of Mechanical Engineering, University of Thessaly

Member: Dr. Costas Papadimitriou
        Professor, Department of Mechanical Engineering, University of Thessaly

Member: Dr. Georgios Charalampous
        Assistant Professor, Department of Mechanical Engineering, University of Thessaly

Date Approved: [7/10/2022]

Acknowledgements

I would like to express my gratitude to my supervisor, Professor Spyros A. Karamanos for his valuable assistance during the implementation of this thesis. I am also very thankful to Dr. George E. Varelis for the development of the idea of this thesis and for his guidance throughout the writing process.

Moreover, I would like to thank the members of the examination committee of my dissertation Professors Costas Papadimitriou and Georgios Charalampous for carefully reading my work.

Lastly, I am very grateful to my friends and family whose moral support played a significant role during these five years of my studies.

FLOW INDUCED VIBRATIONS IN PIPING

Lydia Lymperopoulou

Department of Mechanical Engineering, University of Thessaly

Supervisor: Dr Spyros A. Karamanos
Professor of Structural Mechanics

ABSTRACT

Since pipe systems are so widely utilized in daily life, issues and breakdowns are highly likely to arise. Especially, when components are present which create abrupt changes in flow, turbulence is occurring. In the case of pipe elbows, the pipe curvature creates unstable flow conditions with the most important being the pressure pulsation. As a result, piping starts to vibrate as well, leading to severe fatigue cracking issues. This phenomenon is called Flow Induced Vibrations and is a result of the fluid and structure interaction. In this thesis, numerical analysis was conducted using the commercial program ANSYS Workbench. The simulation model created was described as well as the loading conditions enforced. Results were taken for two geometrical models with different diameter and curvature. Furthermore, the boundary condition of the inlet velocity changed values and its effect on the system response was studied. Primary focus was given on the mechanical response of the pipe in terms of its displacement, the stress accumulation and the interacting forces. Diagrams for all these variables were displayed and commented. The ovalization of the cross-section was noticed. Fatigue stress analysis was also conducted for both geometrical models. It was concluded that geometrical characteristics play a fundamental role on where the maximum stresses will be occurring. The inlet velocity dictated the amplitude of the vibration which increased gradually with the increase in velocity. Regarding the possibility of fatigue failure, it was seen that all cases were highly likely to suffer from fatigue. Lastly, propositions were made in order to avoid the vibrational phenomena.

Contents

List of Figures

List of Tables

1. INTRODUCTION

1.1. The problem of FIV in piping

The term Flow Induced Vibrations (FIV) is describing the flow-related phenomena of noise and vibrations that appear in many industrial plants. These problems occur due to fluid flow and make it difficult for the facility to run smoothly. Depending on the type of structure or system involved, different disciplines are being used. One of the cases that Flow Induced Vibrations might be found is pipeline systems. Fluid transporting pipe systems mediate the exchange of materials both inside and between organisms and their surroundings. They are common in a variety of sectors, including marine and civil engineering, nuclear and electric power systems, petroleum and chemical processing, human veins and various aspects of everyday existence.

It is easy to see that the fluid force acting on a body in the flow will fluctuate because of flow unsteadiness. In turn, this force, may cause the body to vibrate. In the case of a fluid running through a pipe, under certain circumstances, the flow can exert pressure on the pipe's walls, causing it to deflect. The pipe may become structurally unstable as a result of this displacement [1]. Pressure surges can occur when fluids running through pipes change direction, resulting in both high and low pressures. Low pressures have the ability to cause a pipe to collapse. Reaction forces and resonance frequencies may be determined using structural dynamics and static pipe stress analysis [2].

FIV can be classified according to the type of flow involved. The following flow types, that are of interest, are steady flow, unsteady flow, and two-phase flow. The most often observed scenario for vibration in steady flow is the interaction between fluid and structure leading to increasingly greater vibration amplitudes. In unsteady flow, turbulence forces are the most common source of structural vibration excitation. Because the two-phase flow is a combination of fluids of different densities moving together, the time dependence of the flow momentum functions as a source of excitation for the structure. The variation of pressure in the flow along a pipe can create structural vibration, as well [1].

More specifically, the instability phenomenon of pipes conveying fluid has been studied thoroughly, as well as the dynamic characteristics of the system. The dynamics are known to be sensitively dependent on the natural frequency of the system, the support/boundary conditions and the velocity of the fluid that passes through. In some circumstances, a drop in the natural frequency might be quite crucial. If the pipe's inherent frequency falls below specific thresholds, it becomes prone to resonance and as a result, fatigue failure [3].

However, pipeline systems used in industrial applications are vast and complicated. Therefore, they consist of several long straight pipes and equipment joined by sharp bends. The curved pipe sections are called pipe bends or elbows. Elbows are important parts of pipe networks. They are required to transport fluid from

one location to another, and they, along with the supports, govern the static and dynamic behavior of the structure and fluid [4]. If a fluid is travelling down a straight pipe that bends at some point, the fluid particles will alter their principal direction of motion as a result of the bend. An unfavorable pressure gradient is caused by the curvature, resulting in a drop in velocity near the inner wall. The opposite will occur towards the pipe's outer side [5]. An imbalanced force occurs in the fluid as a result of the pressure gradient and a considerable pressure differential causes vertices in the flow, which cause turbulence and structural vibration. It is obvious that elbows are points of the tubes prone and sensitive to the occurrence of Flow Induced Vibrations [6].

The most common vibration related issue is piping fatigue. Especially in parts of flow discontinuities, like bends, the development of FIV due to internal pressure instabilities can cause fatigue-induced failure. The range of the frequencies that are critical for fatigue development may vary from 20 Hz to 5000 Hz, depending on the geometry and the flow. What determines the response of a system to an applied excitation is the connection between the natural frequencies of the system and the frequency of the excitation. Therefore, many computational tools have been developed to predict a structure's fatigue life estimates, according to the relationship between these two frequencies [7].

1.2. History of FIV research

Research regarding Flow Induced Vibration and generally Fluid-Structure Interaction began in the seventies when the first scientific conferences started to take place. In addition to that, Dr. Robert Blevins published the first textbook in this field in 1977. After he had used it as the title of his book, the term "Flow Induced Vibration" became well-known. FIV phenomena were categorized in the book for the first time, based on two primary flow types: steady flow induced and unsteady flow related. Blevins followed up by publishing a handbook on the frequency and eigenmodes of structural and fluid systems and how they are related to the appearance of FIV. In Germany, Prof. Naudascher wrote a book about the hydraulic forces operating on dams and gates, mostly from the civil engineering and hydraulics perspectives. Also, Padoussis and Li dealt with the issue of axial FIV and have published an important work on the fundamental principles behind coupled fluid–structure oscillations in pipes carrying fluids. In 1980, a committee of the Japanese Society of Mechanical Engineers (JSME) on FIV, led by Prof. Tajima, examined the state of the art in FIV, publishing a report that included numerous examples of flow-induced phenomena in the Japanese industry.

Across the world many conferences have been held over the years. Specifically, since 1990, the " Yayoi research seminar " has been conducted at the University of Tokyo's nuclear test facility to introduce research projects and distribute information about nuclear power plants. At the American Society of Mechanical Engineers

(ASME), the "International Symposium on Fluid–Structure Interactions (FSI), Aeroelasticity, and Flow-Induced Vibration and Noise" is held every four years while a FIV symposium is held at almost every conference of the Pressure Vessel and Piping Division. In Europe, every four years, the "International Conference on Flow-Induced Vibrations" is organized. In Japan, during every JSME conference, a FIV session is held yearly [1].

Conferences that are still taking place today include: the "International Symposium on Fluid-Structure Interactions, Flow-Sound Interactions, Flow-Induced Vibration & Noise" and the "International Conference on Flow-Induced Vibration ". All these events imply that Flow Induced Vibrations is still an "unresolved-open" issue which attracts significant scientific interest.

In the industry, in order to avoid FIV phenomena and address the potential failures the "Guidelines for the avoidance of vibration induced fatigue failure in process pipework" is being widely used. These guidelines were published by The Energy Institute of London in 2008 (second edition). A full description of the mechanisms that cause FIV is provided, as well as methods for coping with the problem in a real-world manufacturing unit [8].

1.3. Scope of this study

As demonstrated previously, the flow dynamics cause Flow Induced Vibration difficulties in numerous engineering structures. Excitation is caused by the production of turbulent flow, leading to unstable loads and consequently vibrations.

The purpose of this study is to examine the oscillations in water-filled pipe systems giving emphasis on the curved pipe sections called pipe bends or elbows. The elbow that is being studied has an angle of 90°. The fluid's change of direction raises concerns regarding the formation of turbulence and, as a result, the structure's troublesome operation. The main goal is to illustrate the phenomenon of Flow Induced Vibrations that appear on pipe bends, to analyze the reasons for its development from a physical and mechanical point of view and investigate the implications on its mechanical response and fatigue resistance.

A numerical analysis was performed for this process. A Computer-Aided Engineering (CAE) simulation was conducted using the ANSYS Fluent software. A Computational Fluid Dynamics (CFD) model was created to simulate the interaction of the water with the surface of the elbow by defining the boundary conditions. In addition, the model employed the principles of the Navier-Stokes equations and the flow's form was tracked and depicted. With the use of the fluid-structure interaction software the CFD model of the water was coupled with the Finite Element Model (FEM) of the elbow simulating the effect the structure and the fluid have on one another. The FEM model was able to predict the mechanical behavior of the pipe

bend, as well as the oscillatory phenomena. Finally, the likelihood of failure from fatigue was examined.

2. THEORETICAL BACKROUND

This chapter will skim through the fundamental concepts that were needed in this thesis, in order to draw the final conclusions. Basic principles of Engineering, such as extended theory of Mechanical Vibrations, and Fluid Mechanics are not mentioned.

2.1. The importance of Natural Frequencies

The oscillatory motion of dynamic systems is called vibration. All bodies with mass and elasticity have the ability to vibrate. On the other hand, every Mechanical system can be modeled as a vibratory system as seen in **Figure 1.** A vibratory system consists of a mass (m), a spring (k), a damper (c) and an excitation (F). Through a source of excitation, energy enters the system. This energy can be stored in the mass in the form of kinetic energy and in the spring in the form of potential energy. The damper is a means of dissipating this energy. When there is no damper in the system it is called, a conservative system and there is no energy dissipation.
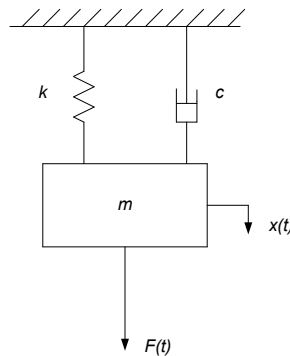
Figure 1: Vibration System of one degree of freedom

The system is initially at rest, in equilibrium position. Assuming the mass is displaced from equilibrium, the system possesses potential energy restored in the spring. When the mass is released, the potential energy of the spring will be transferred into the mass as kinetic energy. This periodic exchange of potential energy into kinetic energy and vice-versa is called vibration, appearing as a periodic motion. The maximum displacement (amplitude) of the mass from equilibrium will not diminish from cycle to cycle. The equation of motion for this case is:

$$m\ddot{x} + kx = 0 \qquad\qquad (1)$$

The rate of energy transfer between two different types of energy storage components, namely the mass and the spring, is described by natural frequency. It is the frequency at which the undamped free response occurs naturally. The natural frequency is implied in this discussion as a system feature. It is unaffected by the

oscillation's amplitude or the initial conditions and is only dependent on the values of *m* and *k*. *M* stands for the mass of the system and *k* for the stiffness of the spring.

$$\omega_n = \sqrt{\frac{k}{m}} \qquad (2)$$

Now, a system with damping is assumed. The damped system will vibrate at a damped natural frequency ω_d, smaller than ω_n. This is as a result of the system's motion being resisted and slowed down by viscous friction:

$$\omega_d = \omega_n \sqrt{1 - \zeta^2} \qquad (3)$$

Where ζ is the damping ratio $\zeta = \frac{c}{2\sqrt{km}}$. The damping force continually dissipates energy leading to a continual decrease in the maximum displacement on each cycle of motion. In other words, the amplitude decreases exponentially with time and the vibration fades.

If an excitation force is applied to the system, this will move as a result of the initial conditions and the excitation. If the force is simply harmonic:

$$F(t) = F_0 \sin(\omega t + \theta) \qquad (4)$$

where F_0 is the amplitude of the excitation, ω is its frequency such that $\omega = \frac{2\pi}{T}$ and θ is its phase. It is noted that ω is independent of the natural frequency of the system ω_n. The system will tend to vibrate at its natural frequency as well as follow the frequency of the excitation as reflected in **equation 5**.

$$m\ddot{x} + c\dot{x} + kx = F(t) \qquad (5)$$

The general solution of this equation is the sum of the homogenous solution (for F=0) and the particular solution that is specific to *F*. In a damped system, the steady-state response for a periodic excitation is defined only by the particular solution since, because of damping, the free response does decay leaving only the forced response as the long-term response.

If the system has no damping and the frequency of excitation corresponds with or is near to the natural frequency, the homogenous response is significant. A resonance state arises when the system is undamped and the excitation frequency matches the natural frequency. The vibrations of an undamped system can continue at their natural frequency without any energy input. As a result, every energy input will be used to raise the vibration's amplitude, and at resonance this amplitude will increase with no limit. In a mechanical system, resonance is a catastrophic phenomenon that can result in failure or unintended significant displacements.

For a system with damping some of the energy input is lost in the damper. As a result, at resonance the amplitude of the vibrations will not be increased with no boundaries, but it will be significantly magnified [9],[10],[11].

2.2. Fatigue

Small amplitude oscillation does not cause permanent damage to materials. But if the amplitude is increased the material will start to suffer from fatigue. The cyclic oscillation hardens the material and causes damage in the form of accumulation of disturbances. Thus, any system that is repeatedly loaded is susceptible to fatigue failure. Fatigue failure depends on the amplitude of the cyclic stresses and the total number of cycles.

Fatigue can be categorized as low-cycle and high-cycle. In examples of low-cycle fatigue, it is typical behavior for the stresses to exceed the yield strength and for failure to occur in a few loading cycles. In high-cycle fatigue the stresses remain elastic but form cracks which cause failure. However, for this to happen many more cycles are required.

For low-cycle fatigue a sample is loaded in a cyclical manner around a mean value and the number of cycles required for fracture is recorded. The data is presented on an S-N curve where S ($\Delta\sigma$) is the stress range from maximum to minimum value and N (N_f) is the number of cycles until failure. Usually, stress changes in the form of a sinusoidal wave with an amplitude of:

$$S_a = \frac{\sigma_{max} - \sigma_{min}}{2} \tag{6}$$

These curves are mostly based on experimental data and are used to determine fatigue life. For many materials there is a fatigue limit. Fatigue limit or endurance limit indicates that below this value an unlimited number of loading cycles can be applied to a material without inducing fatigue failure. Thus, it can be concluded that the endurance limit is analogous to the yield stress used in strength design [12].

2.3. Turbulent Flow through pipes

A pipe's internal flow can be classified as either laminar or turbulent. When the flow is laminar, there is only one velocity component parallel to the pipe's direction. On the contrary, when the flow is turbulent the predominant velocity component is perpendicular to the flow axis, but it is unsteady (chaotic) and accompanied by randomly behaving components in the other two axes. This chaotic flow motion is so fast that it cannot be seen with the naked eye.

$$\vec{V} = \{u\}\hat{\imath} + \{v\}\hat{\jmath} + \{w\}\hat{k} \tag{7}$$

Turbulent flow fields are characterized by a 3D vorticity $\zeta = \nabla \times \vec{V}$ due to the rotation of each fluid element

In order to study flows through pipes it is necessary to introduce the non-dimensional Reynolds number (Re) which expresses the ratio of inertial forces to viscous forces and characterizes the flow as laminar or turbulent.

$$Re = \frac{\rho \cdot D \cdot V}{\mu} \qquad (8)$$

For a flow through a round cylinder, if Re is greater than 4000 the flow is turbulent. If it is smaller than 2100 the flow is laminar. The transition between laminar and turbulent flow is described in **Figure 2,** along with the dependence on Reynolds number.
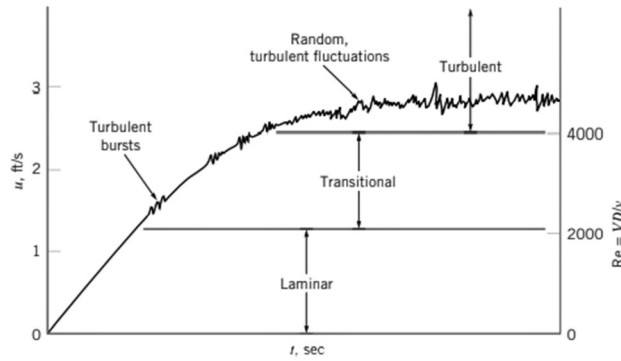
Figure 2: Transition from laminar to turbulent flow in a pipe [13]

Generally, a fully developed flow through a pipe of standard diameter is driven either from gravity or from pressure difference or from both. For horizontal pipes gravity is negligible and the pressure difference Δp between cross sections is equal to the force produced from the viscosity of the fluid. For non-developed flows the fluid can be accelerating or decelerating. The force equilibrium indicates the existence of a pressure gradient $\frac{\partial p}{\partial x}$.

In order to express these phenomena, it is necessary to use the Navier Stokes equations. However, the non-linearity of these equations, due to the turbulent flow, makes it very hard to find analytical solutions. As a result, non-dimensional numbers are used:

$$\frac{\Delta p}{\frac{1}{2}\rho V^2} = \varphi \left(Re, \frac{l}{D}, \frac{\varepsilon}{D} \right) \qquad (9)$$

where $\frac{\Delta p}{\frac{1}{2}\rho V^2}$ is the pressure coefficient and $\frac{\varepsilon}{D}$ the relative roughness. This equation shows that pressure loss in turbulent flow is dependent not only from the viscosity but also from the density of the fluid and the roughness of the pipe [13].

2.4.   Steel Pipe Bends

2.4.1. Pipe Bends or Elbows

Piping systems rarely travel in a straight line from process to process. Several components like turns, joints etc. are being used. Elbows are a type of pipe bend (curved pipe parts) capable of changing the direction of a fluid running inside a pipe. A 90-degree elbow can change the direction of the fluid up to 90°.

The geometry of an elbow is depicted in **Figure 3**. The inner section of the elbow is called intrados and the outer section is called extrados. The flank is the area at 9 and 3 o'clock near the mid axis. It is located between the extrados and the intrados, and it is the elbow's critical location. D is the pipe diameter, t the pipe thickness and R the radius of curvature. Elbows generally can be classified as short radius and long radius. Short radius elbows are elbows with ratio $\frac{R}{D} \leq 1.5$ while long radius are the ones with ratio $\frac{R}{D} \geq 1.5$. In the case of cold bends, which are manufactured in a cold bending machine by plastically bending a pipe joint, the radius of curvature can be up to 10 times bigger the pipe diameter ($R>10D$).
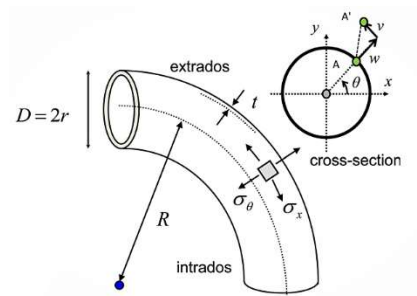
Figure 3: Elbow Geometry [14]

2.4.2. Flow characteristics

Losses in pipe flows are expressed as a drop in total pressure. Pipe bends cause greater pressure drop compared to a straight pipe due to the flow separation near the inner side of the bend and the secondary motion of the fluid. And that is because, in straight pipes, pressure losses are a result only of frictional effects. The significance of the flow separation is determined by the curvature radius of the bend. On the other hand, the secondary flow is generated by the imbalance of the centrifugal forces due to the pipe's curvature [13]. The curvature will provide an unfavorable pressure gradient, with an increase in pressure leading to a reduction in velocity along the curved wall and the converse happening on the outside of the pipe [15]. Secondary flow is depicted on **Figure 4.**
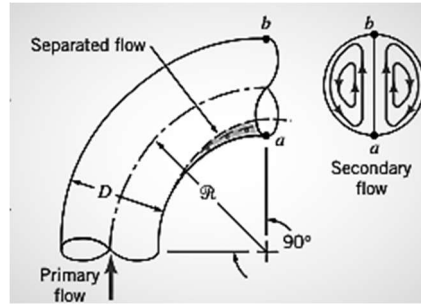
Figure 4: Flow structure on a 90° elbow [13]

It is crucial to define the non-dimensional radius of curvature of the bend as $\frac{R}{D}$. R is the radius of the bend curvature and D the diameter of the pipe. This ratio determines the behavior of the secondary flow. If $\frac{R}{D}$ is greater than 1.5 (long radius elbows) then, the secondary flow consists of two oppositely spinning vortexes. Meanwhile, the primary flow is distorting and shifting away from the bend's center as the fluid in the pipe's center is being moved towards the outside and the fluid near the pipe wall is returning to the inside in the opposite direction. If $\frac{R}{D}$ is less than 1.5 (short radius elbows), a flow separation occurs right after the bend and the flow turns unstable [16].

Dean [17] was the first to provide a theoretical solution of the fluid motion through curved pipes. That's why the two oppositely spinning vortexes are also called Dean vortices and they are the illustration of the secondary motion. The non-dimensional Dean number De is a measure of the point that these secondary vortices will occur. The Dean number quantifies the intensity of the secondary flow and is a comparison between centrifugal and viscous forces.

$$De = Re\sqrt{\frac{D}{2R}} \qquad (10)$$

Curved pipe turbulent flow has proved to be more challenging than laminar flow. The slower flowing fluid was mostly contained to a thin shedding layer close to the pipe walls where the axial velocity was at its highest at the pipe outside wall. In the bend, a radial pressure gradient is generated and transmitted upstream into the inlet pipe through the wall boundary layer. A way to measure the system's losses is by using the loss coefficient. Loss coefficient is a dimensional number that evaluates the velocity changes due to external parameters. In elbows, the upstream and downstream tangents have a significant impact on the loss coefficient. In addition, friction played a fundamental role in pressure drop [15].

A great number of experiments were carried out by Ito [18] and empirical formulas for the bend-loss coefficient were given. The total bend-loss coefficient is given by

$$k_t = \frac{\Delta h_t}{V^2/2g} \tag{11}$$

where Δh_t is the total pressure head loss chargeable to the pipe. The experimental results showed that along the outer wall (extrados) there was a rise in pressure, accompanied by a corresponding fall in pressure along the intrados. It was also noted that it was needed a length of 50 diameters after the elbow, in order for the pressure to retrieve the upstream tangent. The empirical formula that Ito produced through the experiments for the bend loss coefficient was

$$k_t = 0{,}00873 a f_c \theta \, \frac{R}{r}, \quad for \, Re \left(\frac{r}{R}\right)^2 \le 91 \tag{12}$$

$$k_t = 0{,}00241 \alpha \theta \, Re^{-0{,}17} \left(\frac{R}{r}\right)^{0{,}84}, \quad for \, Re \left(\frac{r}{R}\right)^2 \ge 91 \tag{13}$$

where f_c is the friction factor, α is a numerical coefficient and θ the deflection angle.

The first to study analytically how the secondary flow oscillates was Hawthorne [18]. If vorticity $\zeta = \nabla \times \vec{V}$, the component of the vorticity in the direction of the flow is responsible for the secondary flow. To perform his analysis, Hawthorne, assumed a surface of constant total pressure p_0 with streamlines and vortexes and called it Bernoulli surface. The angle between the Bernoulli surface and the direction of the normal flow was called φ. The eddies of the secondary flow were scaled by the parameter ξ. If qdA the constant volume flow, the secondary circulation will be an analogy of $\frac{\xi}{q}$. After some mathematical calculations, Hawthorn retrieved the following equation

$$\left(\frac{\xi}{q}\right)_2 - \left(\frac{\xi}{q}\right)_1 = -2 \int_1^2 \left| grad \, p_0/\rho \right| \sin \varphi \frac{d\theta}{q^2} \tag{14}$$

where dθ is the angle between tangents to the streamline at points arc length ds.
When it enters the elbow, the secondary flow, creates a spiral motion and as a result the pressure becomes distorted. The above equation now gives approximate results because the distortion of the surfaces is not negligible. An initial flow with uniform pressure and stable profile of velocity enters a bent at angle $\varphi = \frac{\pi}{2}$ so that a secondary flow is produced. It was proven that the acceleration of the flow will be directed towards the center due to the pressure distortion. If this distortion is a twist of an angle a then, angle φ will now be $\varphi = \frac{\pi}{2} - \alpha$ and equation 14 now becomes

$$\frac{\xi}{q} = -2 \int_0^\theta \left| grad \, p_0/\rho \right| \cos \alpha \frac{d\theta}{q^2} \tag{15}$$

It is assumed that ξ is uniform over the cross section, the circumferential velocity at the outer diameter $v = -\frac{1}{4}\xi d$. The ratio $\frac{v}{q}$ shows the linear displacements of the particles of the flow where q is the velocity normal to the cross section. In an elbow with turn $d\theta$ the angular displacement will be da. Therefore, the linear displacements

can also be written roughly as a product of $d\theta, r, da$. Where r is the distance of a fluid particle from the elbow center so it becomes

$$\frac{v}{q} = \frac{d}{2r}\frac{da}{d\theta} = \frac{d}{2}\int_0^\theta \frac{|grad\, p_0/\rho|}{q^2} \cos\alpha\, d\theta \qquad (16)$$

In order to simplify the problem, Hawthorn assumed a linear velocity profile with $U_{max}=U$ and $U_{min}=0$ so

$$\frac{gradp_0/\rho}{q^2} = \frac{1}{q}\left|gradq\right| = \frac{U}{qd} \qquad (17)$$

This equation alongside with velocity q being constant justifies the assumption that the vorticity is uniform in a cross section. Hawthorn, for simplicity, followed the behavior of the fluid particles with the highest pressure. After some mathematical calculations and simplifications, he concluded that for pipes with radius of curvature large compared to their diameter, the equation (17) becomes

$$\left(\frac{d}{R}\right)\frac{d^2\alpha}{d\theta^2} = \cos a \qquad (18)$$

which corresponds to the equation of motion for a pendulum of length L and angle a.

$$\left(\frac{L}{g}\right)\frac{d^2\alpha}{dt^2} = \cos a \qquad (19)$$

Hence, the fluid in the elbow will oscillate between $a = 0$ and $a = \varphi$ with a period of $T = 2\pi/\sqrt{R/d}$. Hawthorne, confirmed his analytical equations with experimental data. The good convergence showed that the effect of friction is not so important outside the boundary layer.

Over the last years, many numerical studies were conducted giving emphasis on the secondary flow inside an elbow. Numerical results were compared with experimental data and how the secondary flow is affected by Reynolds number and the radius of curvature. Jongtae, Yadav and Seungjin [20] analyzed the effect of dissipation in the flow structure and the swirl intensity. The existence of the eddies in the middle of the elbow decreased the velocity in the center leading to an increase in the velocity near the wall. At the same time, the velocity profile remained symmetrical. The uneven velocity needed a length of 10 diameters to be diffused by turbulent dissipation. Furthermore, it was noted that for Re numbers between 50.000 and 200.000 flows exhibit similarity and velocity profiles flatten. For the two counter-rotating swirls swirl intensity I was used to express their power and strength. I had a minimum dependence on Re number and was decreased exponentially with turbulent dissipation downstream of the elbow. High values of the radius of curvature produce a quicker turbulent dissipation.

Kaldy and Ayala [21] performed a quantitative assessment comparing secondary flows through bends when standard parameters were changed. In this way, they observed the bend behavior and how it was impacted by Re and curvature. As Reynolds number and velocity increased the flow became more turbulent. It was noticed that when Re decreased the two counter-rotating vortices changed their

position and moved away from the elbow walls. That was the outcome of the influence of the inertial forces. The size of the eddies decreased alongside Reynolds number because for higher Re flow structures were more resilient to changes. On the other hand, it could be said that for greater radius of curvature the fluid had more time to develop in the elbow and absorb the consequences of the centrifugal forces. However, in reality, smaller radius of curvature vorticity grew bigger which was caused by the existence of centrifugal acceleration.

Lastly, Crawford, Spence and Cunningham [22] simulated secondary flows with five different numerical turbulent models. They used these models to predict the structure of the flow and the pressure loss. They concluded that computational simulations do not always converge with experimental results due to flow separation, strong pressure gradients and high streamline curvatures. The numerical results showed a linear pressure loss when in fact the decrease was oscillatory. The flow rebounding off the pipe walls resulted in oscillations in pressure as the flow readjusted in the axial direction.

2.4.3. Mechanical Behavior

Elbows have a much better mechanical behavior compared to straight pipes. They are more flexible and can accommodate high stresses and strains. Their flexibility is why they are resistant to thermal stresses and expansions, can absorb external loads and it generally controls the piping systems' dynamic response. Pipe bends are defined by a severe cross-sectional deformation called "ovalization". Despite their good performance, they are regarded as critical elements for the systems' structural stability since the plasticity is expected to be concentrated on them.

Von Karman [23] firstly introduced an analytical solution for the radial displacement of arbitrary point of the elbow cross section w. He used a doubly symmetric trigonometric function as

$$w(\theta) = a\cos 2\theta \qquad (20)$$

In the absence of pressure, a relationship between the moment m and the curvature k was suggested, with m and k being the non-dimensional values.

$$m = \frac{\pi k}{\eta} \qquad (21)$$

where $\eta = \left(\frac{1}{1-\frac{9}{10+12\lambda^2}}\right)^{-1}$ the flexibility factor and $\lambda = \frac{Rt}{r^2\sqrt{1-v^2}}$ dimensionless parameters defining geometry shown in **Figure 3**. For the case of internal pressure, Rodabaugh and George [24] introduced a more generalized form of the von Karman equations assuming uniform deformation. They expressed the total deformation with the radial and the tangential displacement through series of doubly symmetric trigonometric functions as

$$w(\theta) = \sum_1^\infty a_n \sin 2n\theta \qquad\qquad (22)$$

$$v(\theta) = -\sum_1^\infty 2a_n \cos 2n\theta \qquad\qquad (23)$$

where a_n the corresponding generalized coordinates. The solution is obtained by minimizing the potential energy.

The elbow response is controlled by cross-sectional ovalization. Ovalization is the phenomenon of the elbow flattening symmetrically in an oval shape with respect to the plane of bending. The pattern at which the elbow flattens is opposite under opening and closing moments respectively. When out-of-plane bending occurs, cross-sectional flattening appears at 45-deg with respect to the plane of bending. This behavior is schematically explained in **Figure 5**. When assuming elastic behavior, it is indicated that the elbows are considerably more flexible than their equivalent straight pipe. That applies also to the stresses. The flexibility factor and stiffness, reduces exponentially when internal pressure is raised. Moreover, the maximum circumferential stress is higher than the maximum longitudinal stress and does not appear at the bottom or the top of the cross-section. The total maximum deformation of the whole elbow appears in the middle cross section of the elbow. That is the effect of the ovalization of the cross-section. For higher loads, the hypothesis of elasticity cannot be applied due to great displacements and plasticity and non-linearity rules the phenomenon.
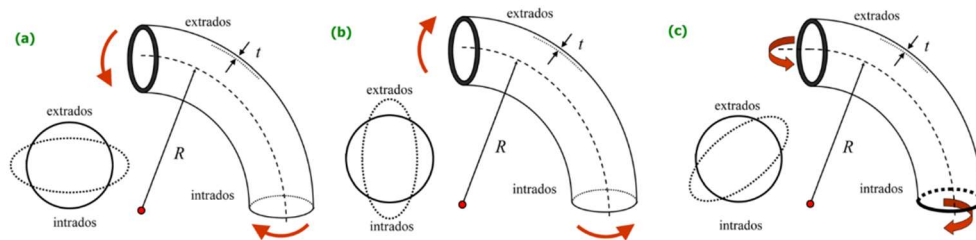

Figure 5: Three types of bending a) closing b) opening c) out-of-plane [14]

Seismic design and analysis have motivated numerus researchers to investigate the matter of pipe bend response under strong cyclic loading. Pipe elbows have been defined as critical components for pipeline systems and are associated with failures like fracture, loss of containment and ratcheting. Ratcheting is called the phenomenon of the substantial accumulation of plastic strain that eventually may lead to plastic collapse [15].

Edmunds and Beer [25] were the first to introduce an analytical solution for short radius pipe bends. They gave the ratchetting rate as

$$\varepsilon^n = 2e_b \frac{2\sigma_1 - \sigma_2}{2\sigma_y - \sigma_2} + \frac{\sigma_2}{2E} - \frac{\sigma_y}{E} \qquad\qquad (24)$$

where σ_1, σ_2 are the follow up stresses and e_b the superimposed bending strain.

Continuing their work, Moreton [26] assumed ratcheting initiation so $\varepsilon^n = 0$ and noted that $Ee_b = \sigma_b$ and $\sigma_2 = \sigma_1/2$ so from equation 24 he extracted

$$\sigma_y = \frac{\sigma_1}{4} + \sqrt{\frac{3}{4}\sigma_b\sigma_1} \qquad (25)$$

He used this equation to calculate σ_y for several different elbows for which experimental values have already been obtained. He contrasted the results of Edmunds and Beer for values of the ratchetting rate and it was evident that the theoretical estimations were two orders of magnitude higher than the measured data. This error may be attributed to testing technique, strain-hardening or residual stresses. In addition, compatibility with the adjacent elements was not taken into consideration since the analysis assumed only an isolated element of material. However, when comparing experimental results with the values retrieved from **equation 24** that is referring to the onset of ratchetting, there is convergence.

Yahiaoui et al [27] tested the ratcheting of stainless-steel and carbon steel elbows under conditions of steady internal pressure and dynamic in-plane bending. The response of the two steels was very different since they have different material behavior with the stainless-steel elbows being able to accumulate higher stresses. Great cyclic strain accumulation and ratcheting was noted. Ratcheting was greater at the hoop direction but the stresses at the axial direction were also substantial at the intrados. Despite those, there was no evidence of plastic collapse.

Numerical studies were also performed by DeGrassi et al. [28]. After carrying material tests to define the mechanical properties, he compared these tests with three different simulation models. The major objective was to select a cyclic plastic hardening model to simulate the ratcheting response of the system. Time history analysis and parametric studies were also conducted. Two linear and one non-linear plasticity model was used to predict the elasto-plastic response. The best match to the test results was given by the non-linear model in terms of estimating the accumulated strain and the total ratcheting behavior.

A large European research program called INDUSE [29] was carried out with collaboration of academic institutions, research centers and industrial partners. The aim of the project was to develop standards which can be applied to seismic design of liquid storage tanks, pressure vessels and piping and enhance the already existent Eurocode guidelines and extend their applicability. Experimental, analytical and numerical extensive studies were made for a number of components like nozzles, branches and elbows. For each component geometric, material and loading parameters were examined. Many papers were published in continuation of the research conducted in the INDUSE program. Specifically, the investigation concerning pipe bends involved experiments under cyclic in-plane bending [30] and corresponding numerical simulations [31], [32].

Varelis et al. [31], [32] performed several experiments for the case of strong repeated cyclic structural loading with and without the presence of internal pressure. The experimental data were compared with a numerical finite element model that simulated the response of the pipe. For the case of nonpressurized elbows [31], the

cyclic loading led to plastic strain accumulation (ratcheting). The ratcheting effect degraded the material while the increasing number of cycles distorted the elbow cross-section. The specimens that were used for the experiments showed that at the cross-sectional flattening occurred at the middle section of the elbow, where the maximum strain appears, and at the locations near the weld. At the same time, the plasticity models that were developed in ABAQUS predicted very well the ovalization and location of cracking which was observed at the elbow crown. It was noted that the hoop strain was much larger than the longitudinal strain verifying the direction of the crack. All tests failed in less than 10^5 cycles indicating low cycle fatigue. The data fitted well with a straight line in the log-log scale resulting to a fatigue failure curve. The already existent design standards seemed to be very conservative since the material can withhold strains up to the plastic region.

Varelis and Karamanos [32] studied the response of the same elbows as the previous study [31] but this time with the presence of internal pressure. The tests exhibited ovalization and failure due to fatigue cracking in the low-cycle fatigue regime. The crack form was the same in all specimens. The finite element plasticity models that were used simulated well the experimental results and showed a dependance of the behavior of the cross-section on the level of the internal pressure. More specifically, when the pressure increased the cross-sectional flattening decreased which indicated the capability of the elbow to endure greater loads. However, the internal pressure produced additional stresses that affected fatigue life. The specimens failed since they cracked at the same critical position (at the elbow crown) because of the ovalization. The higher strains appeared at the hoop direction on the elbow midaxis and therefore the cracks occurred at the longitudinal direction. As in the case of nonpressurized elbows the longitudinal strain range is small compared to the hoop strain range. Nevertheless, the internal pressure made the two comparable and created a biaxial strain field. This biaxial strain field was considered concluding that there is a strain accumulation for increasing loading cycles and failure is always because of fatigue. In order to predict Fatigue Life, Neuber's equation was proposed in addition to other mechanical formulas and design standards. It was also highlighted that the already existent guidelines for process piping cannot be applied in this situation since they predict high-cycle fatigue and the one for pipe elbows gives conservative yet reasonable results.

2.5.   Flow Induced Vibrations-Fluid Structure Interaction

The study of Flow Induced Vibration (FIV) of piping involves the coupling of fluid dynamics and piping structural vibration. The problem is complicated, challenging and highly nonlinear in nature. It can also be described as a Fluid-Structure Interaction problem (FSI). This term refers to the transfer of forces and momentum from a fluid onto a structure and reverse during irregular flow. Excitation mechanisms can be set of by sudden changes in flow and pressure or by mechanical action of the piping. The interaction is expressed in pipe vibration and fluctuations in velocity and pressure of the liquid. A great deal of research activity concentrated on

explaining the mechanical interaction between unsteady flow in piping and the associated vibration of the whole structure.

The basic concept of FSI analysis is that liquid and pipe systems cannot be treated separately in a theoretical analysis. Therefore, interaction mechanisms must be considered. In order to explain the Fluid-Structure Interaction phenomenon, three coupling mechanisms have been proposed as shown in **Figure 6**. Firstly, Poisson coupling is the term used to describe the interaction between the axial motion of the pipe wall and the pressure in the fluid that results from the Poisson effect. Secondly, friction coupling is generated by the shear force between the wall of the pipe and the fluid. And thirdly, junction coupling is triggered by local forces that are out of balance as well as by changes in fluid momentum that arise at pipe bends, T-junctions, or changes in cross-section. In time, domain analysis, coupling strategy involves developing an interaction between two distinct computer codes, one designed for the fluid and another for the structure. In each time-step, data about the output is sent in both directions. This data transfer has been studied by many scientists who expressed concerns for the computational effort needed [33], [34].
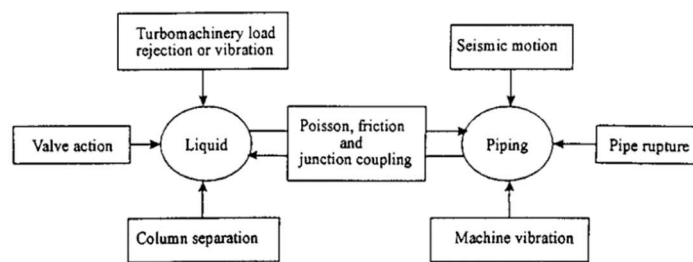

Figure 6: Sources of excitation and interaction between liquid and piping [33]

Each type of Flow Induced vibration can be described and analyzed as different independent flow-related vibration phenomena. It is evident that the mechanisms that cause piping vibration may vary. In particular, these mechanisms can be flow induced turbulence, mechanical excitation from compressors and pumps, pulsation of the process fluid, acoustic excitation from relief and control valves or orifice plates, waterhammer phenomenon, cavitation and lastly, flashing.

When any of the mechanisms mentioned above are present the resulting vibration can be expressed in terms of velocity, displacement and acceleration. It is important, though, to note that the amplitude of those parameters is dependent on the system's natural frequencies as seen in **Figure 7**. Displacement depends on the frequency in a way that results in large displacement at low frequencies and small displacements at high frequencies for the same energy amount. On the other hand, acceleration behaves in a manner that the maximum amplitude appears at the highest frequencies. Velocity presents a uniform profile over the frequency range since it is related to the dynamic stress. Therefore, velocity can be used as a measurement of the vibration conversely

to displacement since the visual observation of the pipework vibration is not a reliable method to evaluate the severity of the problem.
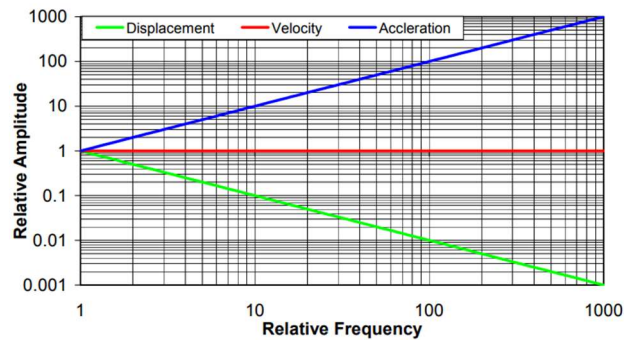

Figure 7: The correlation between the amplitude of the parameters and the frequency [8]

A piping system's response to an applied excitation is affected by the relationship between the system's natural frequencies and the frequency of the excitation. Any structural system will display several natural frequencies which are dependent on how mass and stiffness are distributed on the system. Each natural frequency has a corresponding mode shape. Mode shapes are the unique deflection shapes that components take when vibrating at a natural frequency. The way that the energy of the excitation is distributed separates excitation in two types: tonal and broadband. In tonal excitation, energy is only input at discrete frequencies where in broadband excitation energy is input over a wide frequency range. Therefore, the response of the systems depends on how the excitation frequencies match the natural frequencies response. For tonal excitation, if the system's frequencies match the excitation frequencies a resonant situation takes place. Then, all the excitation energy is capable of stimulating the natural frequencies of the system. In this case, only a small amount of excitation is needed to generate substantial levels of vibration. On the contrary, if the two frequencies do not match, then the vibration still takes place but in a much lower level than when resonance occurs. If the excitation is broadband, then it is highly likely that some natural frequencies will be excited. However, the amplitude of the response is not as high as the resonant vibration case since the energy is shared in a wide range of frequencies [8].

3. PROBLEM DEFINITION

In this chapter the problem is defined as well as the geometric characteristics of the pipe, the mechanical properties of the steel and the fluid.

3.1. Pipe Geometry

In this thesis two numerical models were created to simulate pipe behavior. Both models represent pipe elbows with the same loading conditions but with different geometrical characteristics. Industrial products were examined, a long radius elbow of 6 inches and one of 4 inches. **Table 1** and **2** presents the geometries that were used in the modelling process.

Table 1: Model 1

Pipe inner diameter D_i	142,9 mm
Thickness t	12,7 mm
Elbow Radius- Center to end R_{fillet}	229 mm
Pipe Length L	1200 mm

Table 2: Model 2

Pipe inner diameter D_i	78,3 mm
Thickness t	10 mm
Elbow Radius- Center to end R_{fillet}	304 mm
Pipe Length L	1000mm

3.2. Pipe Material

Choosing the pipe material is an important stage in the pipeline design process. Throughout its functioning, it must tolerate heavy compressive loads, extreme temperatures, and pressures. In the models made, the material was assumed to be Structural steel. Structural steel is a common construction material manufactured from particular steel grades. A popular use for structural steel is extended beams with a profile of a specific cross section. For certain uses, structural steel grades are created with precise chemical compositions and mechanical qualities according to standards. The material properties are listed in **Table 3.** Only elastic properties were introduced since the material is supposed to behave elastically.

Table 3: Properties of Structural Steel

Steel Density ρ	7850 kg/m^3
Young's modulus E	200 GPa
Poisson's ratio v	0.3
Yield Strength σ_y	250 MPa
Ultimate Stress σ_{UTS}	460 MPa

For the fluid running through the pipe, it is assumed to be water with density ρ=997 kg/m³. Gravity is not taken into consideration because the pipe is modeled to be horizontal.

4. NUMERICAL SIMULATION

In this chapter, the modeling of the problem on ANSYS Workbench is presented alongside with the loading conditions that were enforced and the one-way coupling solution. One-way coupling describes the consideration of the ongoing fluid effects on a structural system. The difference with two-way coupling is that the later takes also account of the interaction of the structure to the fluid flow. In the analysis featured in this thesis only one-way coupling is used since there are no significant plastic changes on the pipe cross-section in order to induce changes on the fluid flow.

The simulation model studied the flow inside pipes and the corresponding mechanical response of the material. The same model was applied to the two geometries (Model 1 and 2). The boundary condition of the pipe inlet velocity was the parameter whose influence on the flow and mechanical response was studied. Chapter 4 presents the steps that were followed to procced to the final analysis and explains the basic settings selected. As an example, Model 1 is used.

4.1. Geometries

The two elbow geometries were developed by using the Design Modeler tools. Firstly, it was necessary to create two-dimensional sketches at two different planes. The first plane set the inner diameter of the pipe, while the second plane the pipe length and its direction. To make the elbow curvature, the Fillet tool was used to create the arc that connected the upstream and downstream parts of the elbow. By using the Sweep command, the two two-dimensional sketches became one in a three-dimensional model. The profile of the Sweep was the first sketch, the pipe diameter, and the path were the second sketch, the curvature of the elbow. The elbow complete 3-D geometry as well as the steps that were followed are shown in **Figures 8-9.**
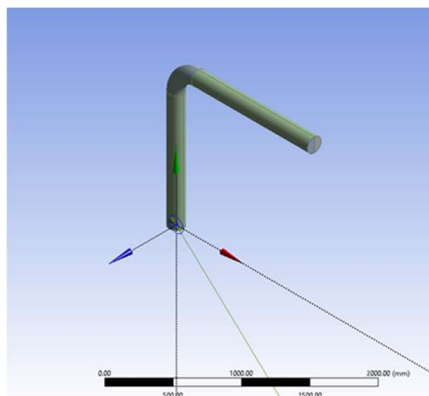
Figure 8: Sketch of the pipe diameter
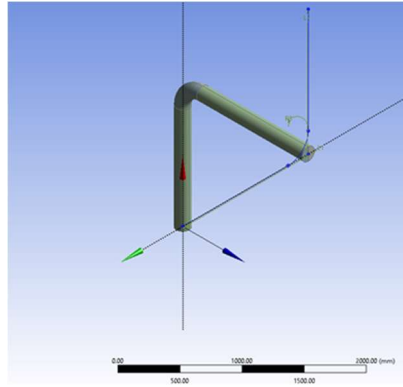
Figure 9: Sketch of the pipe length

The procedure that is analyzed in the previous paragraph basically describes the inner part of the tube since the inner diameter is used. It is easy to understand that this is a way to indicate the volume of the liquid running through the pipe. Because the pipe is a structure whose thickness is significantly smaller than its length it is better to be modeled as Thin Structure. Thin Structures are structures whose thickness is significantly smaller than the other two dimensions. In ANSYS they are modelled as Surface Bodies which in their turn are modeled with the use of shell elements. Shell elements are spatially 3D but geometrically 2D elements since the shell thickness is defined as a cross-section property. Nodes of shell elements have translational degrees of freedom but also have three rotational degrees of freedom. As a result, this allows them to have both membrane and bending behavior. If solid elements are used to mesh Thin Structures, poor results will be observed. To fix this problem the mesh is required to become very fine and as a result the problem will get computationally very expensive.

To do so, another Sweep needs to be done but with the selection of a Thin/Surface as shown in **Figure 10**. The thickness of the tube is not defined in Design Modeler but later in the modelling procedure. In the end, the system consisted of two bodies in total. The first body was the fluid, represented by a solid body, and the second body was the pipe, represented by a surface body.

Figure 10: Defining the pipe as a Surface Body

4.2. Loading Conditions

The simulation began by studying the behavior of the fluid inside the pipe. That was necessary because the movement of the fluid was what created the forces that acted upon the pipe. To do so, a Time History Analysis was performed. Due to the fact that it offers the most accurate characterization of dynamic loads, time history analysis is widely used in stress analysis. It is a step-by-step investigation of a structure's dynamic reaction to a given loading that may change over time. The equations of dynamic equilibrium are solved. If the end of a former analysis is continued, these can be set as initial conditions. The Time History Analysis of the CFD was then transferred to the Structural Analysis.

4.2.1. Fluid Flow (CFX) - Steady State

A steady state analysis was performed at the fluid so that the initial conditions of the time history analysis were set. Steady state flow refers to a flow where the conditions do not change over time. Because the whole geometry from Design Modeler is transferred to Fluid Flow, it is important to suppress the Surface Body that is the pipe. The CFD analysis was performed only on the fluid. The mesh that was built is shown in **Figures 11-12.** It had 428000 elements.
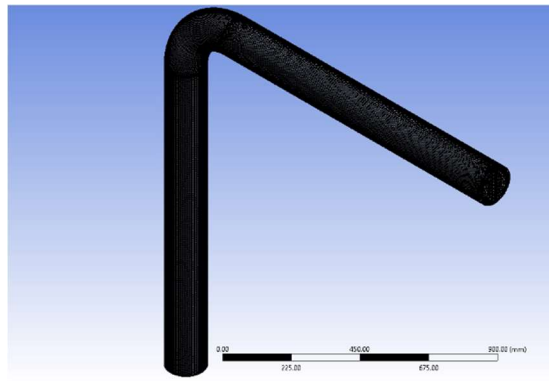
Figure 11:The mesh of the steady state analysis
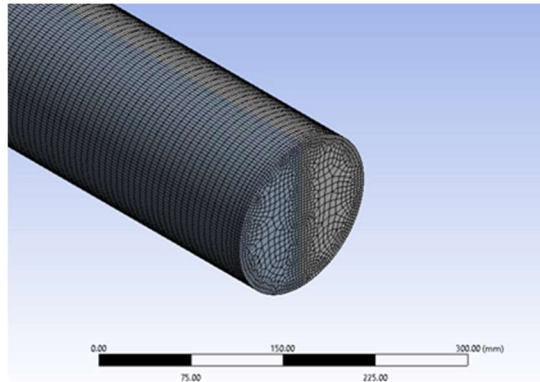
Figure 12: The mesh near the pipe wall

The next step was to apply the settings regarding the characteristics of the flow. The analysis was set as Steady State and the fluid as water following the k-epsilon turbulence model. It is the most popular model being used in computational fluid dynamics (CFD) to visualize flow characteristics in conditions of turbulent flow. The model solves two transport equations. The turbulent kinetic energy k is the first transported variable. The rate ε at which turbulent kinetic energy is dissipated is the second transported variable. Afterwards, the boundary conditions were enforced. At the inlet of the pipe, velocity was set alongside the Turbulence Intensity. For all simulations run, inlet velocity was set at a different value every time . Turbulence intensity represents the root-mean-square of the velocity variations divided to the mean flow velocity. Because 1% is considered low value and 10% high value, a medium intensity of 5% was picked. At the outlet of the pipe relative pressure was fixed at 1 atm. The option of a No Slip Wall was chosen for the pipe wall. When the problem finished running the results were transferred to the Transient CFD analysis as well as the initial Geometry as shown in **Figure 13**. In this way the results of the Steady State analysis were used as initial conditions for the Transient Analysis.
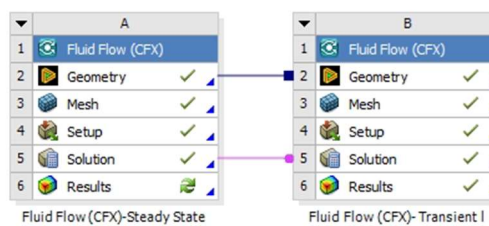
Figure 13: The connection between the two models

4.2.2. Fluid Flow (CFX) - Transient Analysis

The procedure followed when simulating the Transient Analysis was very much like the one presented in the previous chapter. For the same geometry a new mesh was generated. At this stage the mesh was finer because the form of the flow needed to be captured in detail. As seen in **Figures 14-15**, the mesh had 717000 elements and was thicker near the pipe wall so the elements were capable of resolving the boundary layer more accurately. The pipe was suppressed in this analysis and a wall boundary condition was enforced at the location where the pipe wall is.
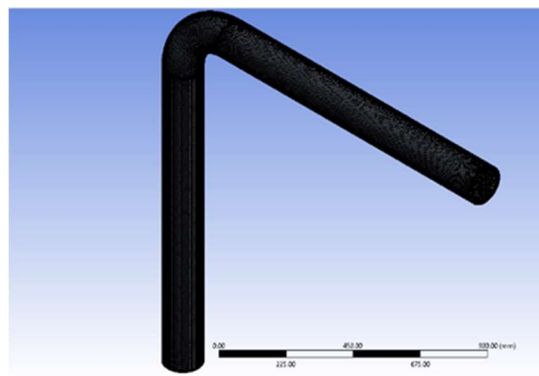
Figure 14: The mesh of the transient analysis
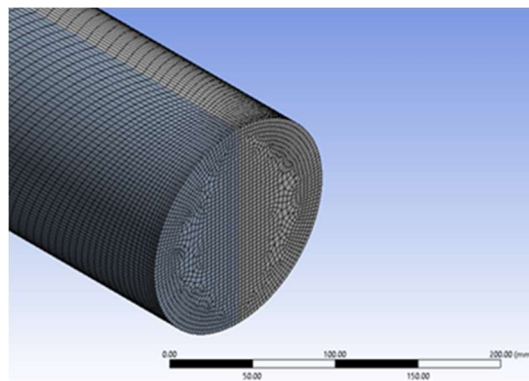
Figure 15: The mesh near the pipe wall

Transient analysis determines a system's reaction over a user-specified time-period. The number of internal timesteps, makes up the entire simulation period, and determines the accuracy of the transient analysis. Hence, at the set-up of the flow characteristics the analysis was chosen to run for a time-period of 1 second and

timesteps were selected at 0.001 seconds. For the fluid the same settings were kept. The boundary condition at the inlet of the pipe was also set. At the outlet relative pressure had the value of 1 atm. In this case, the wall was modeled as No Slip so that the effect of the boundary layer would be more realistic. All boundary conditions in the Transient analysis were selected in the same way as the boundary conditions in the Steady State analysis since the interest focused on flow under stable conditions. Because it was vital to be able to see the behavior of the flow at each timestep, the Output Control was fixed to retrieve results at every timestep.

4.2.3. Transient Structural

The results from the transient CFD were transferred to the structural analysis as shown in **Figure 16**. In this way, the pressure and force fluctuations that occur due to the fluid flow are taken into consideration when calculating the mechanical response of the pipe. The initial geometry was also imported.
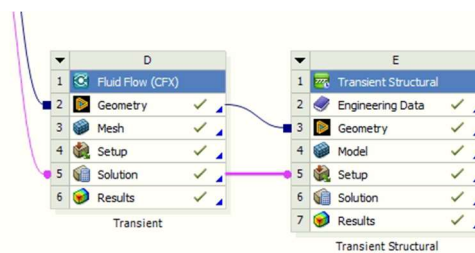
Figure 16: The coupling of results in Transient Structural

However, because in this analysis the pipe is studied, the body of the fluid needs to be suppressed. Moreover, the pipe was modeled as a Surface Body so a value for the thickness needed to be set. Attention should be given to which direction of the pipe the thickness will be added to by checking the correct Offset Type. For this simulation, the inner diameter of the pipe is used to define the geometry so the elements of the pipe should face outward. These settings are presented in **Figure 17.**
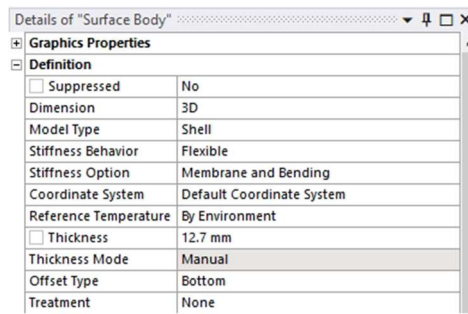
Figure 17: The settings for defining the pipe's thickness

The mesh that was generated for the transient analysis had 13200 elements. Compared to the CFD mesh, much fewer elements are needed because of the shell elements that are capable of saving a lot of computational time. **Figure 18** depicts the mesh of the pipe.
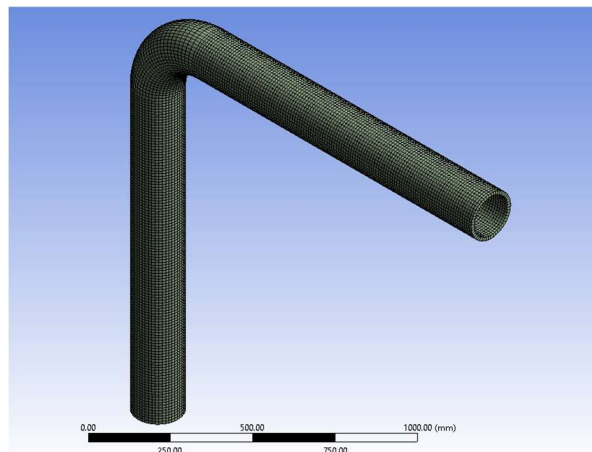

Figure 18: The mesh of the Transient Structural

The next step was to enforce boundary conditions at the ends of the pipe. Remote Displacement conditions were set at both ends. At the inlet, displacement and rotational conditions were set zero apart from the displacement on the y direction. Similarly for the outlet, everything is set zero apart from the displacement in the x direction which is also free. The Analysis Settings were adjusted so as to be compatible with the settings of the CFD, meaning that the total time and the timesteps were the same, as shown in **Figure 19**. At the same time, the pressure profile extracted from the CFD analysis was imported to the mechanical analysis. This is an example of the ANSYS one-way coupling solution. With this method the initial CFD data were automatically transferred and mapped to the Mechanical simulation. The pressure profile being imported was the one on the wall of the pipe since it simulates the Fluid-Structure Interaction and affects the mechanical response of the pipe. **Figure 20** displays the necessary settings for the one-way coupling to be efficiently working and how the tabular data were imported.
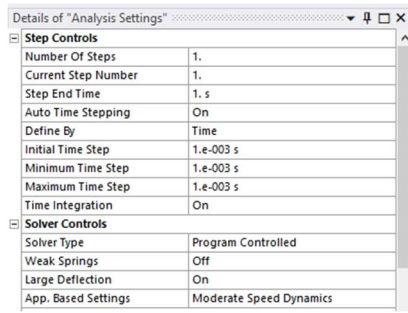
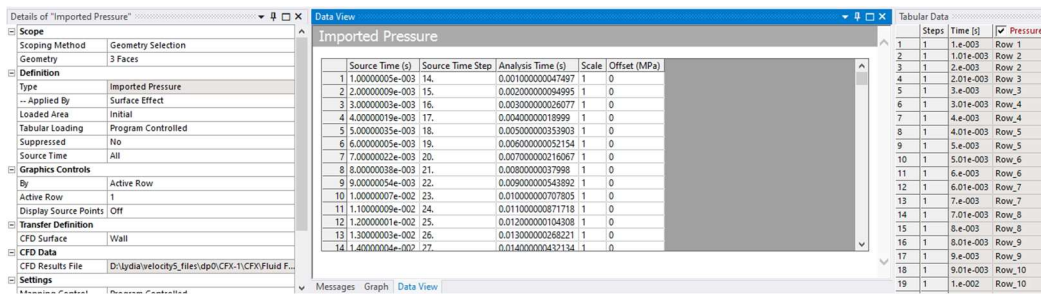*Figure 19: The Analysis Settings of the Mechanical simulation*

Figure 20: The settings and the data imported for the one-way coupling

4.3. Modal Analysis

Understanding the vibration characteristics of mechanical structures may be done with the help of Modal Analysis. It converts the difficult to perceive vibrational signals of excitation and the responses that are observed on a complicated structure, into a collection of easily predictable modal parameters. It includes identifying the natural frequencies and the related mode shapes of a part or structure vibrating freely and demonstrating how various structural components will move in the presence of dynamic loads. Natural frequencies play a fundamental role in a vibrating system since they indicate the frequencies that it will resonate. **Figure 21** illustrates the Modal Analysis tool on ANSYS Workbench.
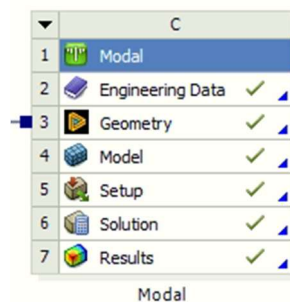
Figure 21: Modal Analysis tool

Modal Analysis's was performed for both models described in Chapter 3. For each case the geometry was imported and a simple mesh was generated. Afterwards, boundary conditions were enforced. The boundary conditions were the same as the ones used in the Transient Structural Analysis, which means Remote Displacement at the inlet and outlet with axes y and x free to move respectively. The results retrieved are listed in **Table 3** for Model 1 and **Table 4** for Model 2. The modes that can be calculated are as many as the degrees of freedom of the system which are the nodal degrees of freedom. However, it is not necessary to calculate all of them and only the first 5 natural frequencies are displayed.

Table 4: Natural Frequencies of Model 1

Modes	Frequencies (Hz)
1.	30.88
2	53.75
3.	82.66
4.	288.44
5.	290.94
6.	401.04
7.	416.31
8.	746.93
9.	783.78
10.	788.52

Table 5: Natural Frequencies of Model 2

Modes	Frequencies (Hz)
1.	17.31
2	34.42
3.	48.52
4.	169.69
5.	170.84
6.	274.72
7.	279.74
8.	506.62
9.	514.24
10.	705.3

For each natural frequency the corresponding eigenmode was created the first three for each model is illustrated in **Figures 22-27**.
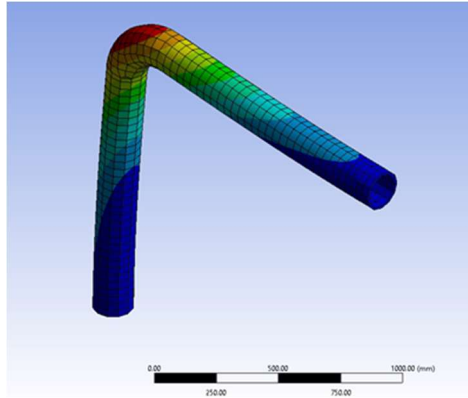
Figure 22: The first eigenmode of Model 1
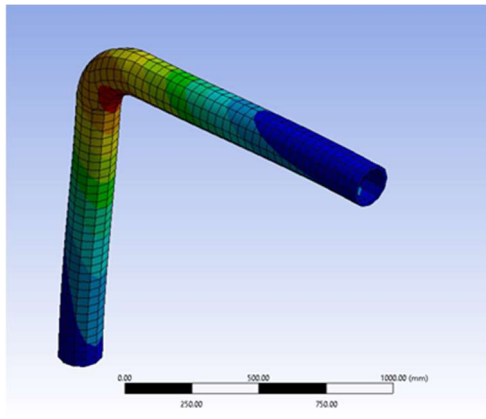
Figure 23: The second eigenmode of Model 1
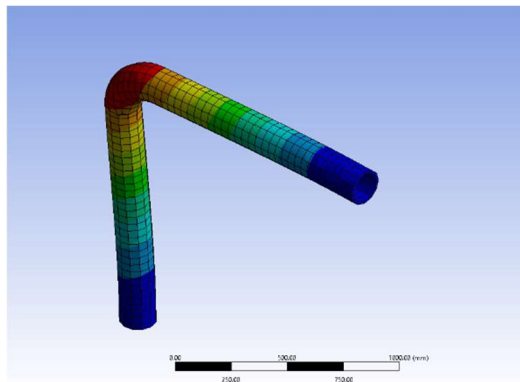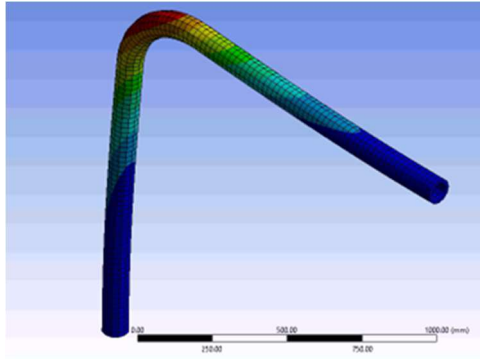

Figure 24: The third eigenmode of Model 1

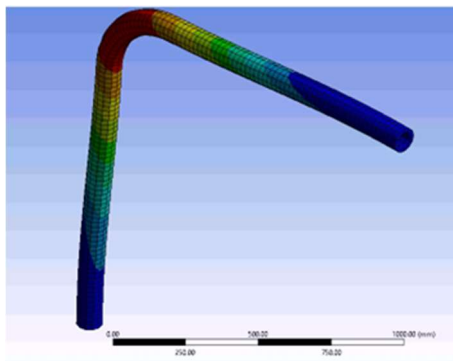*Figure 25: The first eigenmode of Model 2*

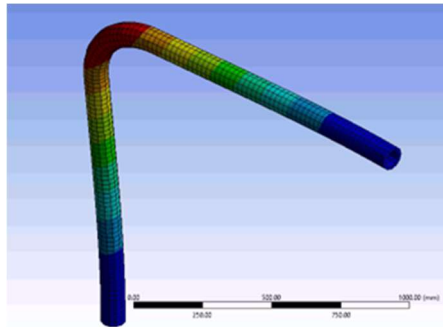*Figure 26: The second eigenmode of Model 2*

Figure 27: The third eigenmode of Model 2

5. RESULTS

5.1. Fluid Flow Representation

The fluid flow analysis simulated accurately the expected behavior of the water inside the pipe. Phenomena such as the pressure gradient and the two opposingly spinning vortexes of the secondary flow could be easily observed. As an example, the schematic illustration of the flow inside the pipe of Model 1 for inlet velocity of 10 m/s is displayed. The same flow characteristics appeared on every simulation run. **Figure 28** depicts the pressure profile on the pipe wall, while **Figures 29-30** the velocity profiles on different timesteps. As anticipated, on the outer wall there was a rise in pressure and a fall on the inner wall. The effect of the boundary layer can be seen clearly as well as the existence of the secondary flow. **Figure 31** shows the two counterrotating eddies.
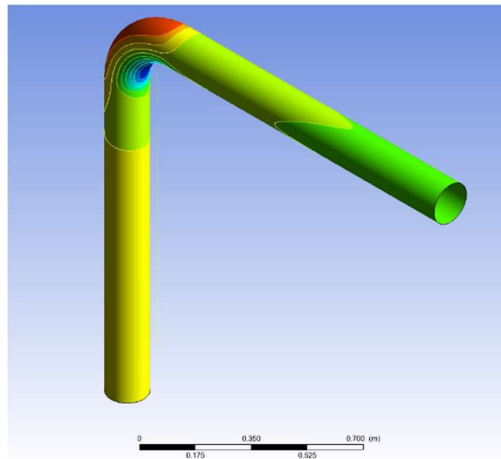
Figure 28: The pressure profile
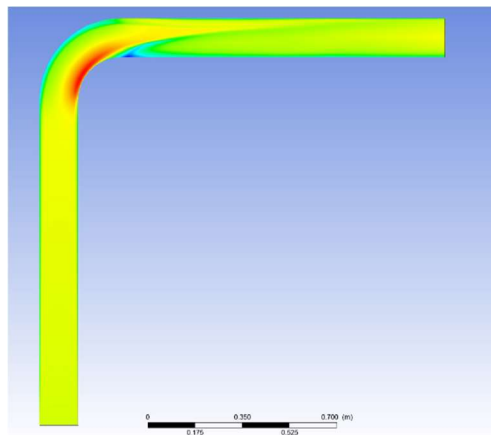
Figure 29: Velocity profile at 0.01 s
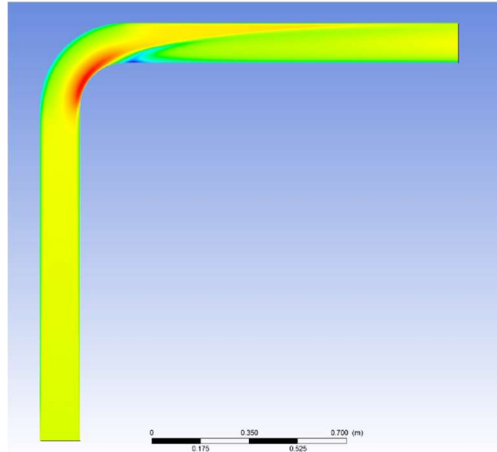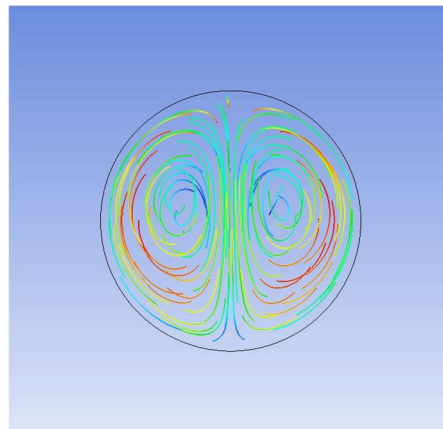
Figure 30: Velocity profile at 1 s

Figure 31: The two spinning vortexes

For both models created, the effect of different values of the inlet velocity was studied. In order to quantify the intensity of the turbulence, Reynolds number was calculated. Reynolds is a function not only of the flow velocity but also of the diameter of the pipe and the properties of the fluid. Therefore, the phenomenon can be presented more accurately. **Table 6** and **7** list the Reynolds numbers calculated for each model and for each inlet velocity. For a flow through a pipe, the critical Reynolds number for turbulent flow is $Re_{critical}=4000$. Consequently, for both Model 1 and 2 the corresponding critical velocity was calculated as $u_{1critical}= 0,025$ m/s and $u_{2critical}=0,046$ m/s. It is easy to see that these values are very unrealistic for an actual piping system, and it is certain that for these geometries turbulence will be occurring.

Table 6: Reynolds numbers for Model 1

u (m/s)	Re
1	160242
5	801210
10	1602421
20	3204843

Table 7: Reynolds numbers for Model 2

u (m/s)	Re
1	87802
5	439011
10	878023
20	1756047

5.2. Structural Response

In this thesis emphasis was given on the dynamic response of a pipe elbow. As it was already mentioned, the parameter that changed was the inlet velocity of the pipe. Special focus was given on mechanical properties such as the Total Displacement of the system, the Equivalent (von Misses) Stress and the Force Reaction at the supports. Results were retrieved for four velocity values u=1, 5, 10, 20 m/s for each model and are displayed below.

5.2.1. Model 1: $D = 142.9$ mm, $t = 12.7$ mm, $R= 229$ mm

As it is mentioned above Model 1 was created with the geometrical characteristics displayed on **Table 1.** For each value of the inlet velocity, results for the Total Displacement, Equivalent Stress and Force Reaction are collected and compared to one another. The diagrams and corresponding photos are presented here.

Total Displacement

Total Displacement describes all results for displacement of the relevant model in three dimensions (X, Y, and Z). It is the resultant vector of the displacement in each direction.
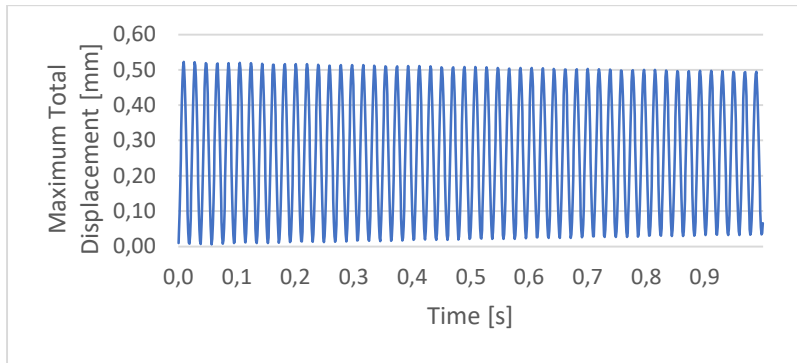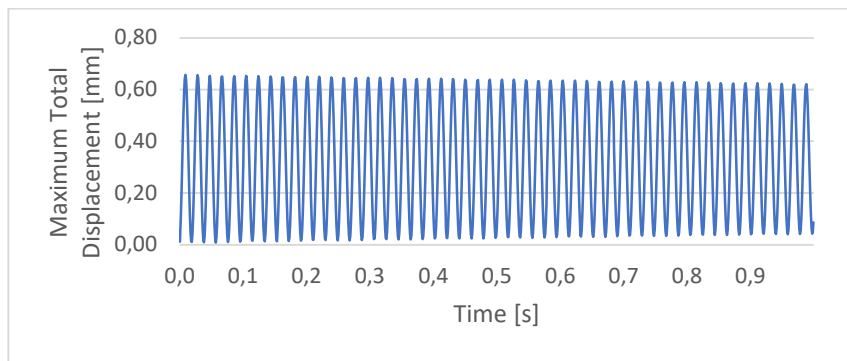
Figure 32: Maximum Total Displacement for u=1 m/s
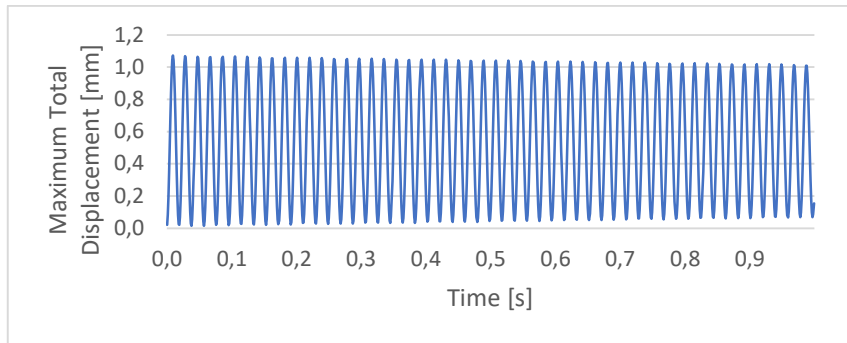

Figure 33: Maximum Total Displacement for u=5 m/s

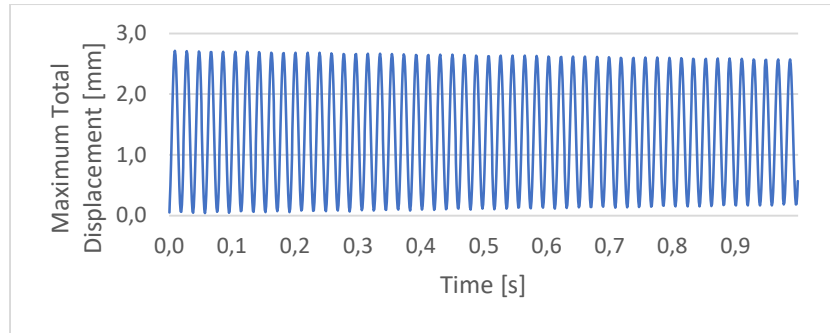*Figure 34: Maximum Total Displacement for u=10 m/s*

Figure 35: Maximum Total Displacement for u=20 m/s

Figures 32-35 illustrate the values of the maximum total displacement calculated on the elbow part at each timestep, for the duration of one second. The values exhibit instability in the form of oscillation. In **Figures 36-37** the representation of the direction of the displacement in space is illustrated. Highest levels of displacement appear on the intrados, the curved part on the inside.
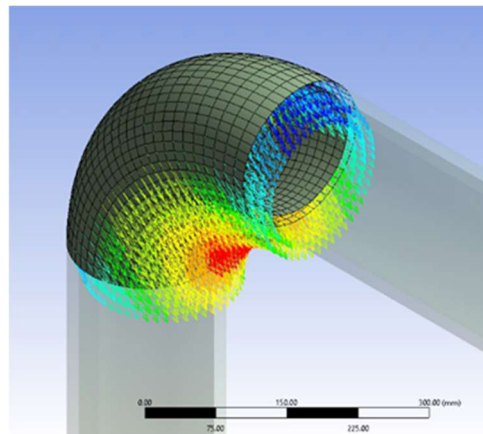
Figure 36: Schematic representation of the direction of deformation
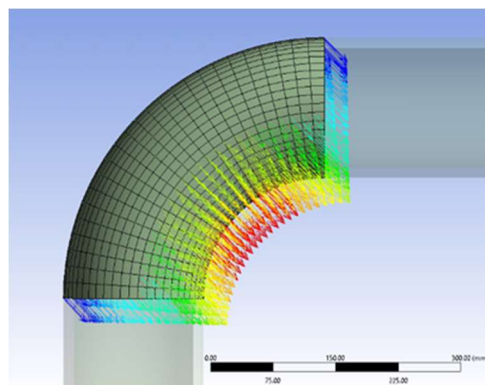

Figure 37: Schematic representation of the direction of deformation

Another way to see the direction of the nodes' displacement is by retrieving the Directional Displacements results on each axis. As an example, the response of Model 1 for inlet velocity u=1 m/s is displayed in **Figure 38**. It can be dictated that in the z direction displacements are very small, indicating that the problem is two-dimensional. Also, the displacements on the x-axis and the y-axis are relatively comparable in terms of their absolute values. However, they occur in opposing directions since on the x-axis they take positive values while on the y-axis they take negative values. The same behavior was exhibited for every simulation run.
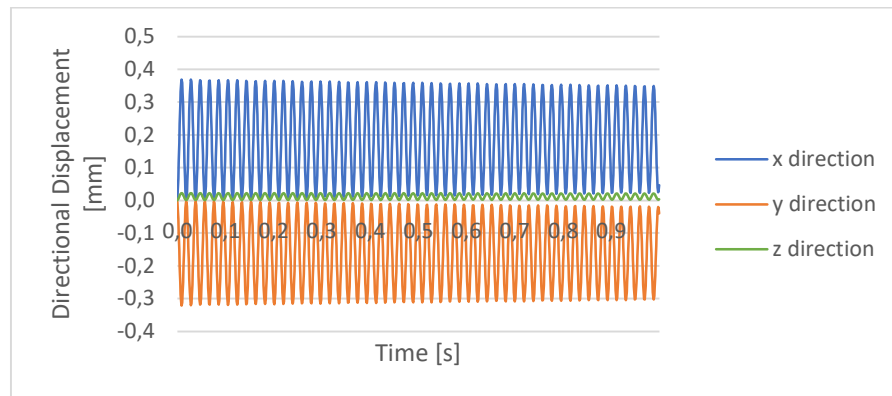

Figure 38: Directional Deformation

Equivalent Stress

The Equivalent von Mises Stress is used to express the stress tensor that is describing the state of the stresses in one value. It is commonly used as a scalar indicator determining failure of a material, since it is a non-directional general stress.
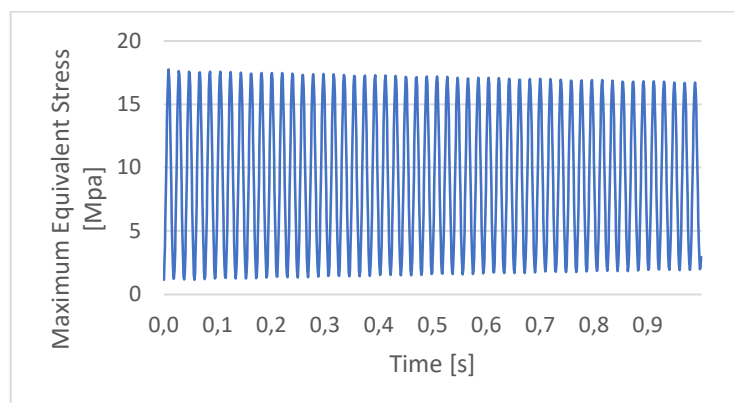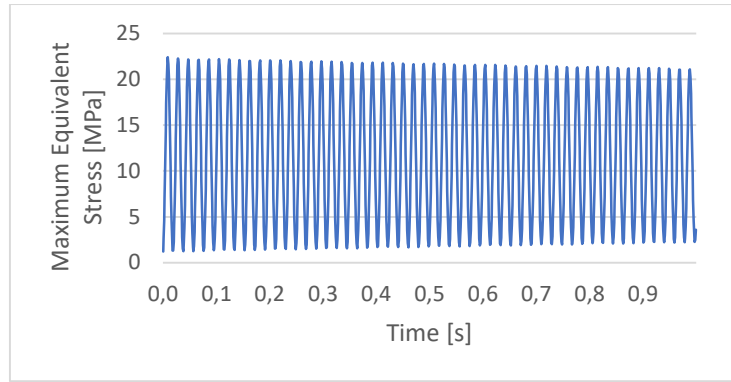

Figure 39: Maximum Equivalent Stress for u=1 m/s
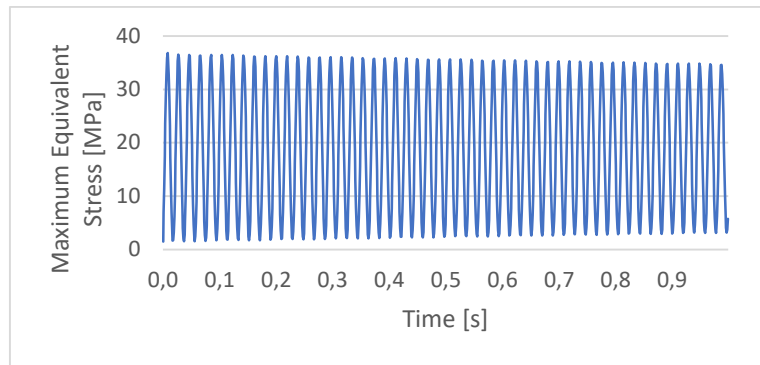
Figure 40: Maximum Equivalent Stress for u=5 m/s

Figure 41: Maximum Equivalent Stress for u=10 m/s
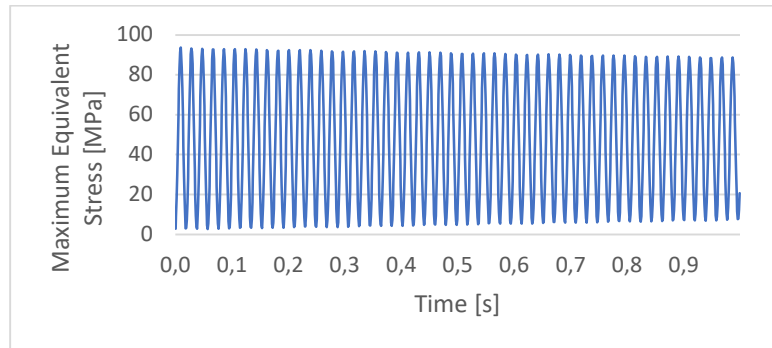

Figure 42: Maximum Equivalent Stress for u=20 m/s

Figures 39-42 display the maximum Equivalent Stress only on the elbow part. For each timestep between 0 s and 1 s a value for the Equivalent Stress on each node is calculated. The vibrational response is also visible and the amplitude of the oscillation increases continuously with the increase in fluid velocity. The maximum of these values is what is presented below. The nodes that are the most stressed are, as expected, those on the elbow flank as it can be seen in **Figure 43**. This is an effect of the elbow ovalization.
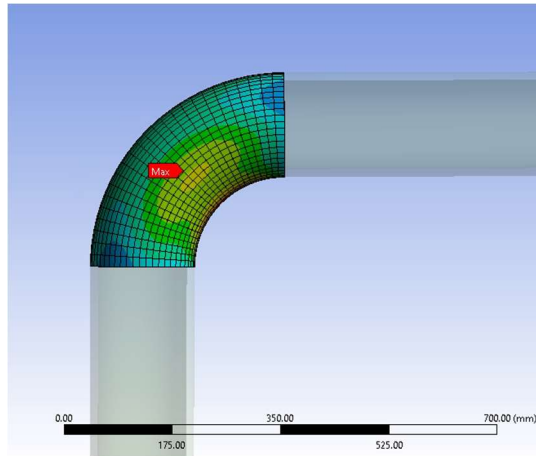
Figure 43: The node that is stressed the most on the elbow part

It is important to note that for the whole pipe structure created the highest stresses appear on the edges where the supports are placed. This is also an expected situation since the supports prevent the free movement of the pipe as displayed in **Figure 44**.
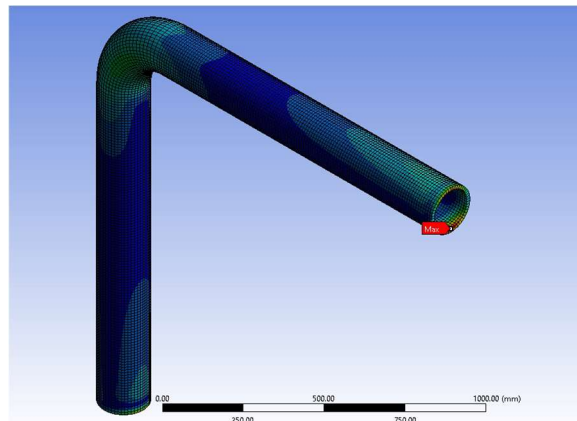

Figure 44: The node that is stressed the most on the whole pipe

Force Reaction

The Reaction Force generated by the resistance of the support to the fluid flow was calculated as seen in **Figures 45-46.** The force was required for the support to prevent the displacement of the tube due to the momentum of the fluid. Once more, the pressure gradient led to the force fluctuation. It is anticipated that the vibrational force is transferred to the support and is highly likely to create a vibrational problem on the support system as well.
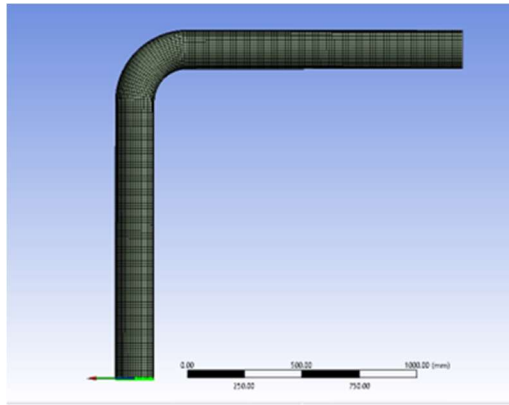
Figure 45: Force Reaction on the inlet support
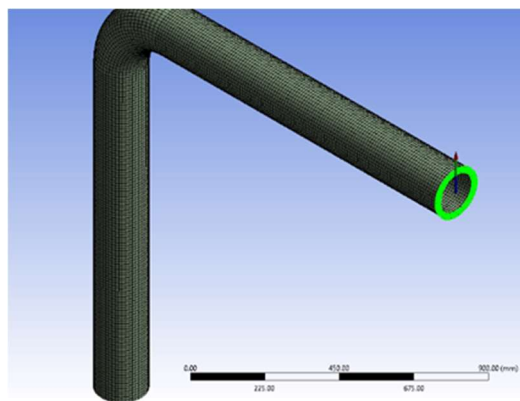

Figure 46: Force reaction on the outlet support

In **Figures 47-50**, Total Force Reaction stands for the net force produced on the supports. It was observed that both supports had equal values for the total force so the diagrams only for the support on the inlet is displayed. This behavior is explained better in **Figures 51-52.**

Figure 47: Force Reaction at u=1 m/s
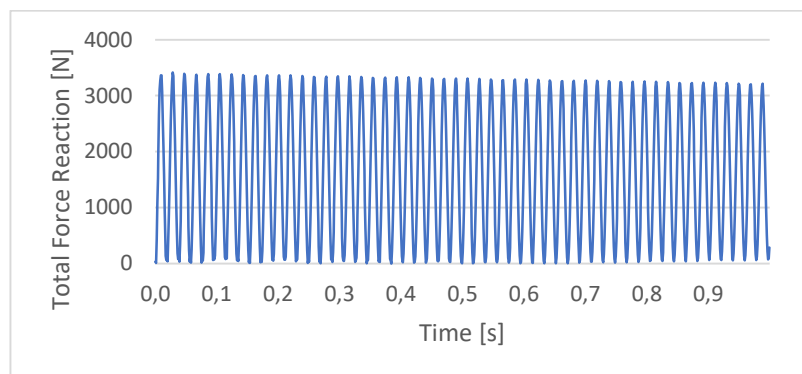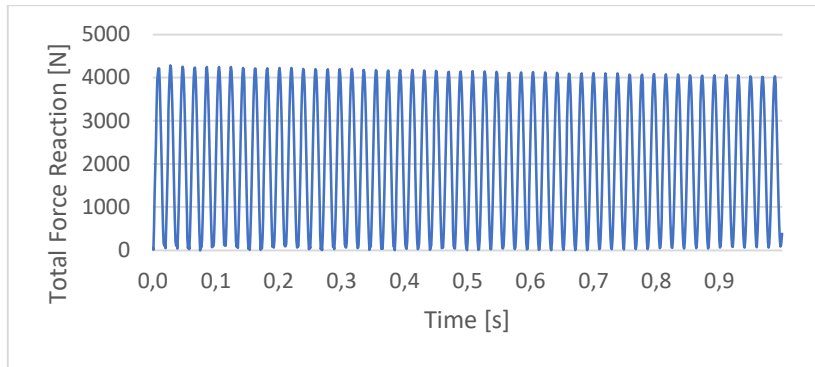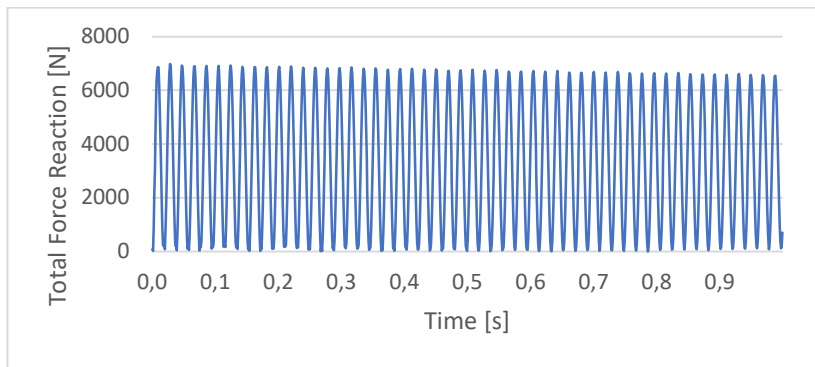
Figure 48: Force Reaction at u= 5 m/s
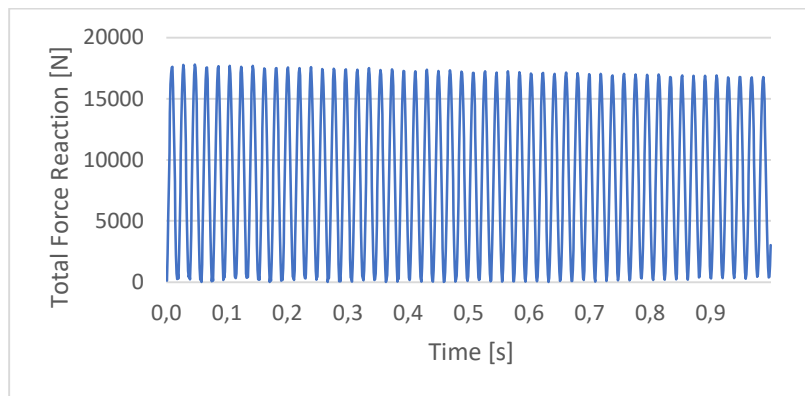

Figure 49: Force Reaction at u=10 m/s

Figure 50: Force Reaction at u=20 m/s

In order to understand how the forces acted upon both supports, the net (total) force reaction was decomposed along the three axes, and the direction which had the greatest effect was observed. In **Figures 51-52,** Model 1 for u=1 m/s is used as an

example. Firstly, it should be noted that the force reaction on the inlet and outlet had the same absolute values. However, on the inlet, forces exhibited negative values and the component on the x direction appeared to have the main effect. On the other two directions the forces obtained zero values. At the same time, on the outlet, the values were positive and the force on the y-axis was the one displaying the main impact. On the other two directions the forces also had zero values. This was an anticipated result corresponding to the boundary conditions enforced on the pipe ends. The direction of the forces justified the opening and closing motion of the elbows.
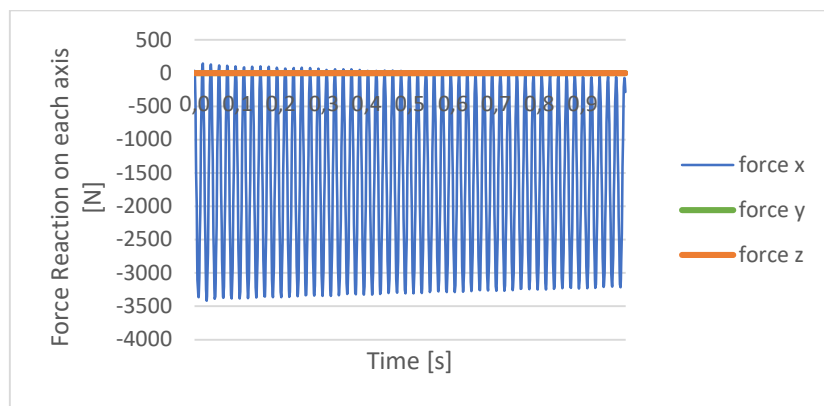
Figure 51: Components of the net force on the inlet
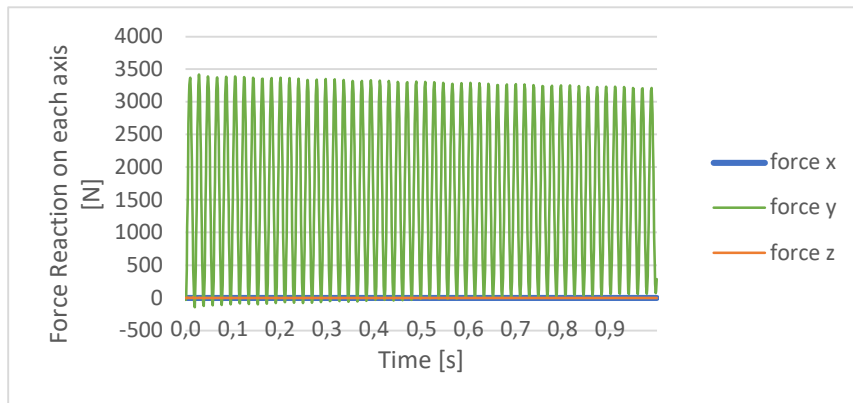
Figure 52: Components of the net force on the outlet

Vibration Mitigation- Added Support

As a way to reduce the oscillations, two fixed supports were placed in the middle of the straight pipes, at x=500 mm from the pipe ends, as seen in **Figures 53-54**. The same simulation as before was run and as an example the case of inlet velocity *u*=5 m/s was used.
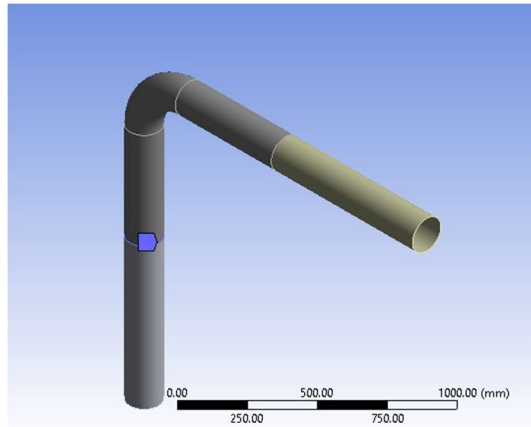
Figure 53: Fixed support on the left side
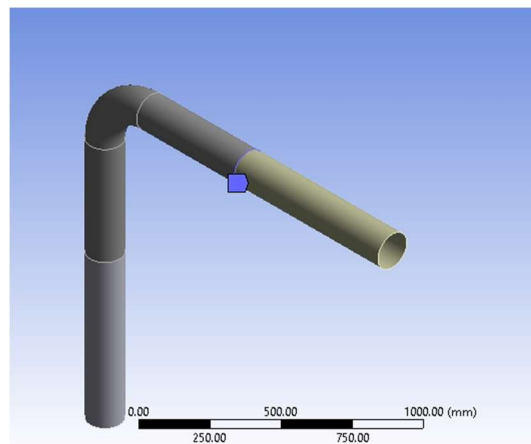
Figure 54: Fixed support on the right side

In the diagrams set out below it can be seen that the fixed supports had the anticipated effect. The oscillations faded out by the end of the time analysis as it is shown in **Figures 55-57**. It is interesting to note that the Force Reaction on the edges of the pipe was zero. On the contrary, the Force Reaction on the fixed supports was stabilized at a constant value.
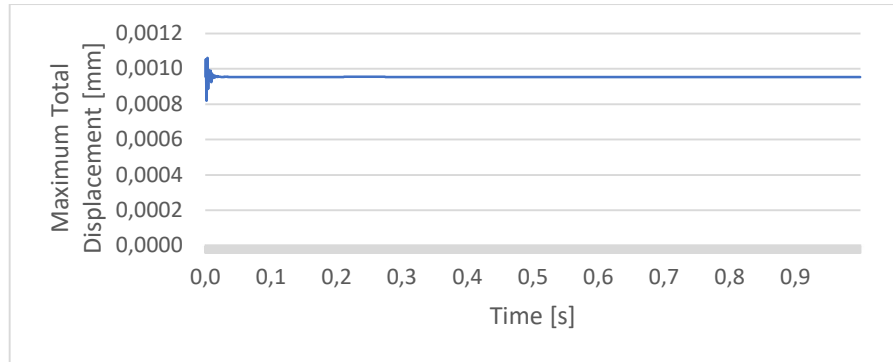
Figure 55: Total Displacement when two fixed supports are placed
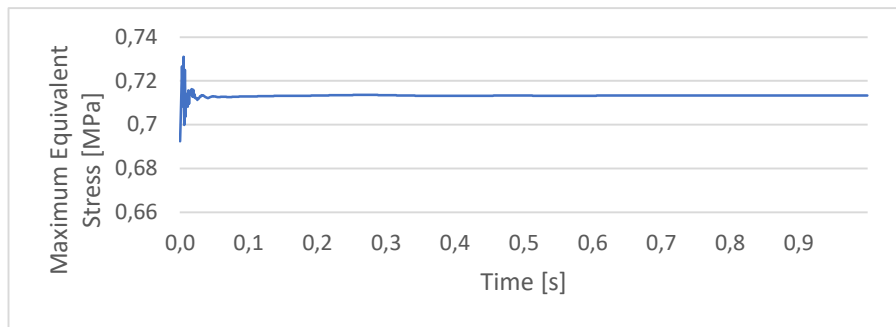
Figure 56: Equivalent Stress when two fixed supports are placed
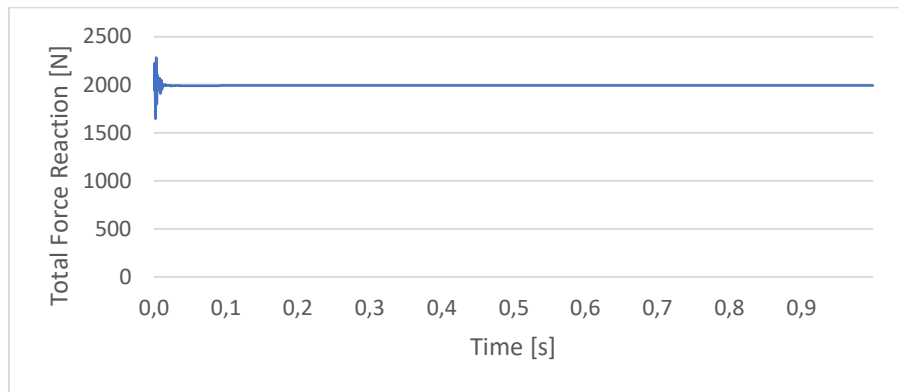
Figure 57: Force Reaction at the location of the two fixed supports

5.2.2. Model 2: $D = 78.3$ mm, $t = 10$ mm, $R = 304$ mm

Model 2 was created with the geometrical characteristics of **Table 2**. The numerical model as well as the loading conditions enforced were the same as in Model 1. Diagrams of the Total Displacement, Equivalent Stress and Force Reaction are listed below.

Total Displacement

The results of the Total Displacement of Model 2 are shown in **Figures 58-61**. The values for each timestep also exhibited vibrational response. The amplitude increased proportionally with the increase in input velocity.
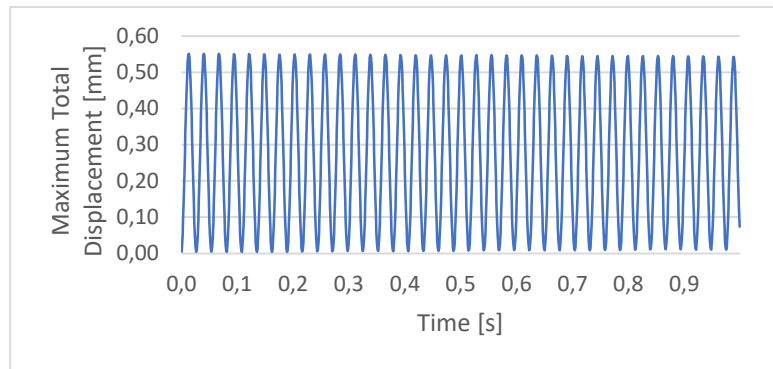
Figure 58: Total Displacement at u=1 m/s
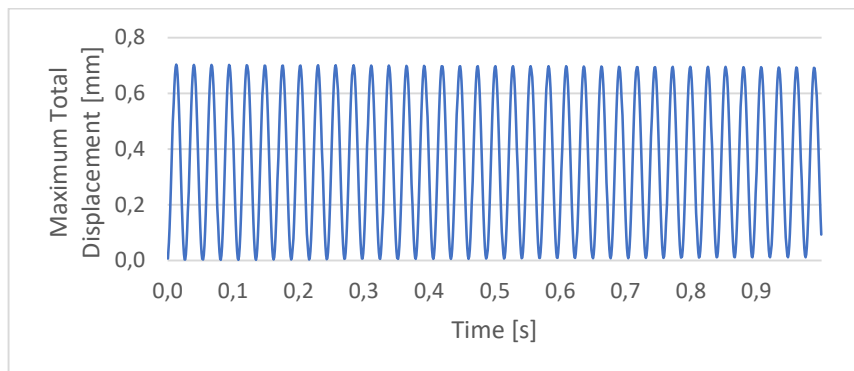
Figure 59: Total Displacement at u=5 m/s
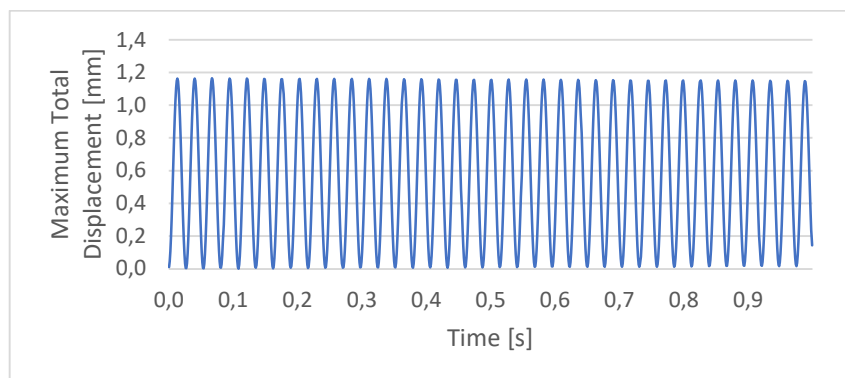
Figure 60: Total Displacement at u=10 m/s
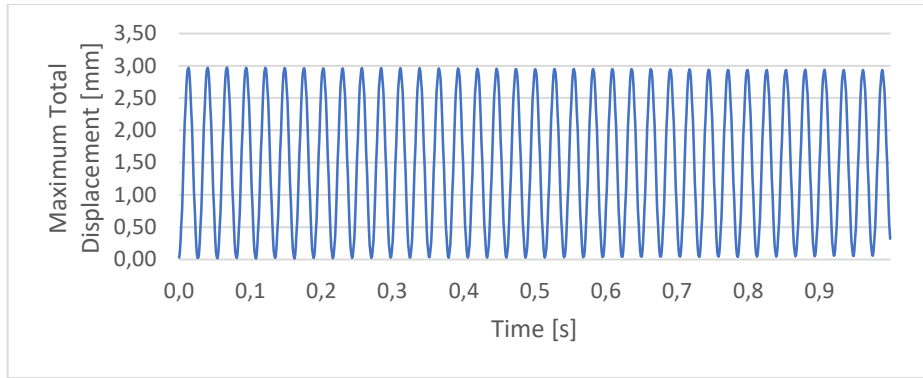
Figure 61: Total Displacement at u=20 m/s

In **Figures 62-63** the direction of the displacement is illustrated. It is also visible that the maximum value appears on the intrados of the elbow.
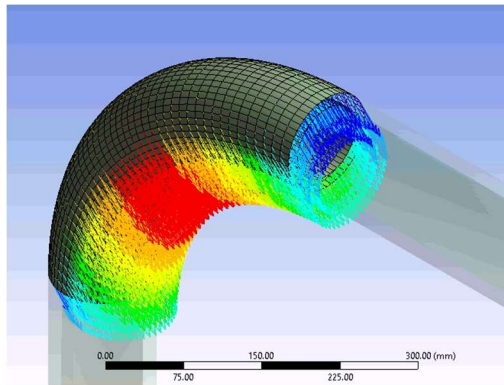
Figure 62: Schematic representation of the velocity direction
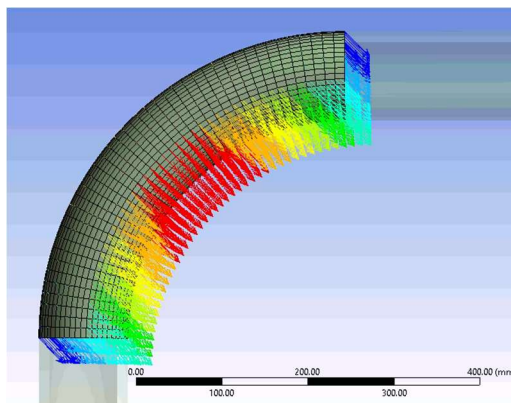
Figure 63: Schematic representation of the velocity direction

Equivalent Stress

As regarding the values for the Equivalent Stress, the corresponding diagrams for each inlet velocity are given in **Figures 64-67.**
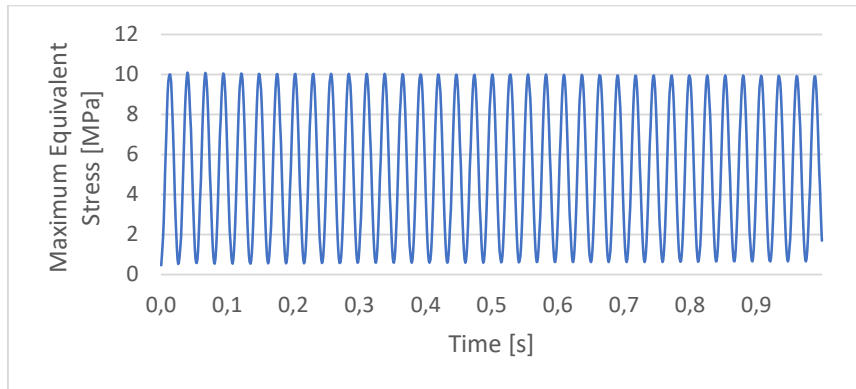
Figure 64: Equivalent Stress at u=1 m/s
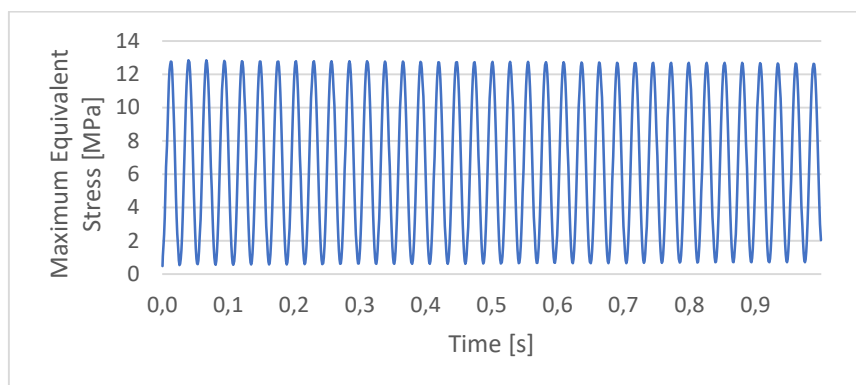
Figure 65: Equivalent Stress at u=5 m/s
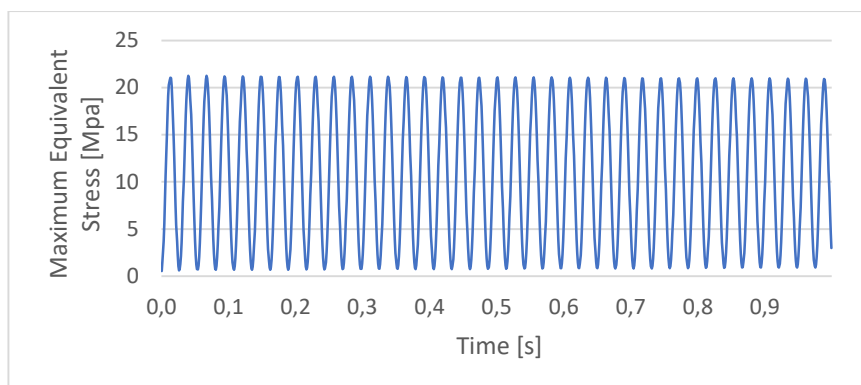
Figure 66: Equivalent Stress at u=10 m/s
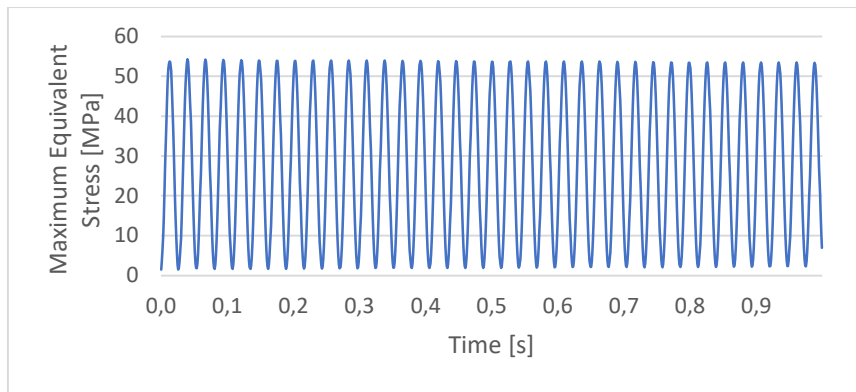
Figure 67: Equivalent Stress at u=20 m/s

An important observation is the location of the maximum Equivalent Stress. It can be seen in **Figure 68** that the nodes at the intrados and extrados accumulate the higher stresses. This is a behavior exhibited by pipes when the strains are very small making them behave like a beam subjected to bending. Ovalization is very small in this case.
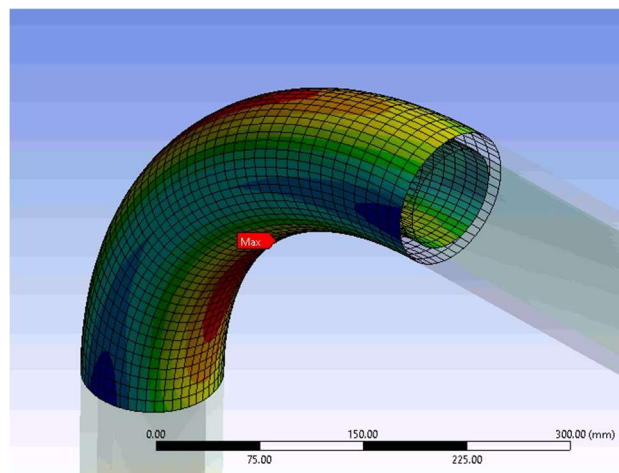
Figure 68: The node that is stressed the most

Force Reaction

Figures 69-72 present the oscillating behavior of the Force Reaction. The Force was calculated on the supports at both ends of the pipe. The component on the axis that was free to move had zero value.
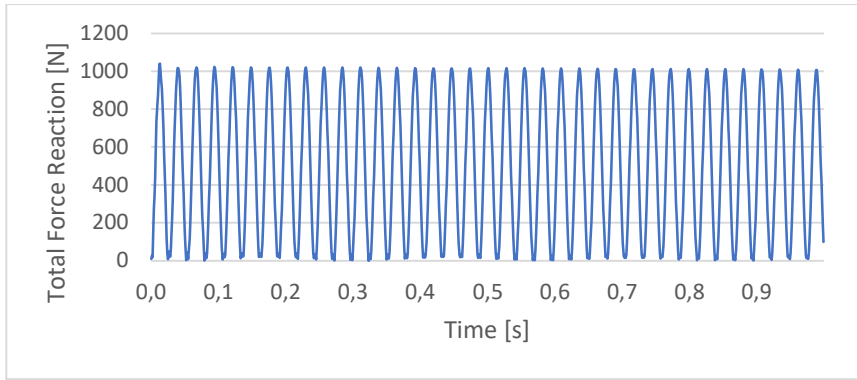
Figure 69: Force Reaction at u=1 m/s
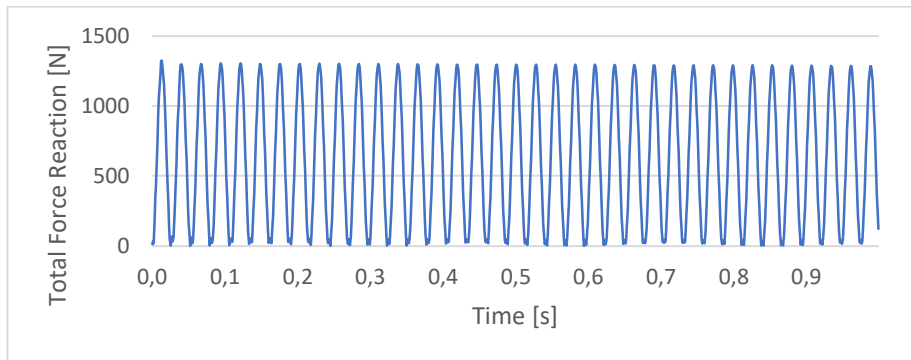
Figure 70: Force Reaction at u=5 m/s
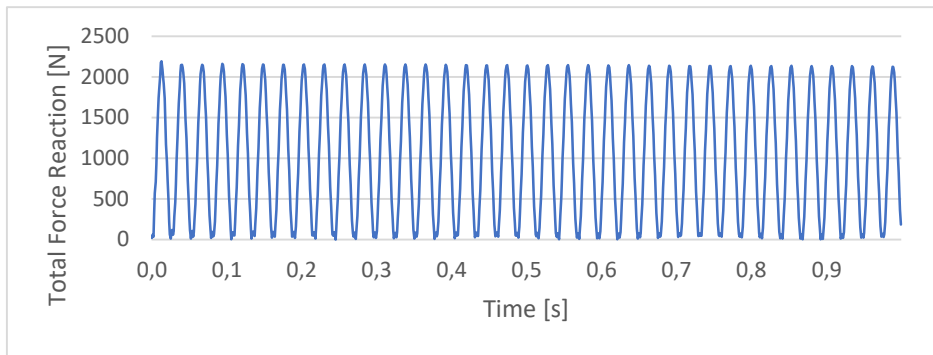
Figure 71: Force Reaction at u=10 m/s
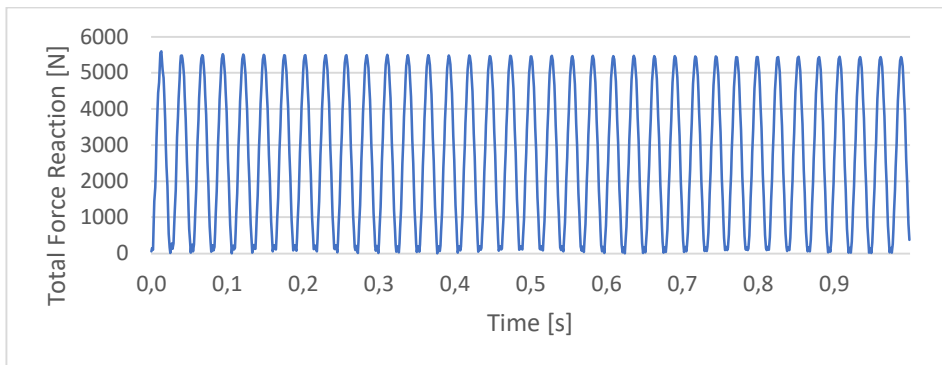
Figure 72: Force Reaction at u=20 m/s

5.3.   Frequency of the excitation

If the number of the complete oscillations performed by a body to the total time interval is the frequency of the vibration then:

$$f = \frac{N}{\Delta t} = \frac{Number\ of\ vibrations}{time} \qquad (26)$$

Using this formula and from data retrieved from the diagrams of section 5.2. the frequency of excitation can be calculated for every loading condition studied. It was seen that the frequency was independent of the inlet velocity. So, for Model 1 it was calculated as $f_1 = 52\ Hz$ and for Model 2 $f_2 = 37\ Hz$. The corresponding periods were $T_1 = 0,019\ s$ and $T_2 = 0,027\ s$. It is observed that for smaller diameter and greater radius of curvature the frequency of the excitation is smaller and fewer oscillations take place during the same amount of time.

5.4.   Resonance

When the frequency of an applied periodic force is equal to or nearly equal to the natural frequency of the system, resonance occurs. This means that the amplitude of the response is enhanced. A dynamic system's vibrations will have a greater amplitude when an oscillating force is applied at its resonant frequency than when the same force is applied at other, non-resonant frequencies. This is an effect of the storage of vibrational energy.

Through the analysis carried out in this thesis, it can be concluded whether or not resonance occurs in the system. For that to be done, the natural frequencies must be compared to the frequencies of the excitations. In Chapter 5.4.2 the frequencies of the excitation were calculated as $f_1 = 52$ Hz and $f_2 = 37$ Hz corresponding to the two models. In addition, in Chapter 4.3 the results of the modal analysis were listed. From **Tables 4** it can be observed that for Model 1 the second natural frequency (53.7 Hz) is almost equal to the frequency of the excitation. At the same time, from **Table 5** it can be retrieved that for Model 2 the second natural frequency is also very close to the frequency of the excitation. Therefore, resonance exists and the amplitude of the response has been magnified. The pipes will be deformed in a manner similar to the second eigenmode as seen in **Figures 23** and **26.**

5.5.   Fatigue Life Estimate

When a material undergoes repeated stress cycles over a specific stress range, an S-N curve is used for the evaluation of the fatigue life of the components and the number of cycles until failure. The standard used in this analysis was ASME pressure vessel and piping code, section III division 1. The vertical axis consists of stress values and the horizontal axis of Number of cycles until failure. **Figures 73-74** show the recommended curve used to estimate fatigue life and its corresponding tabular data. It is observed that if a line is drawn parallel to the x-axis at the point where the curve ends the endurance limit S_e is determined. In this case the endurance limit is retrieved as S_e=40 MPa which means that for lower stress values there is no fatigue damage.
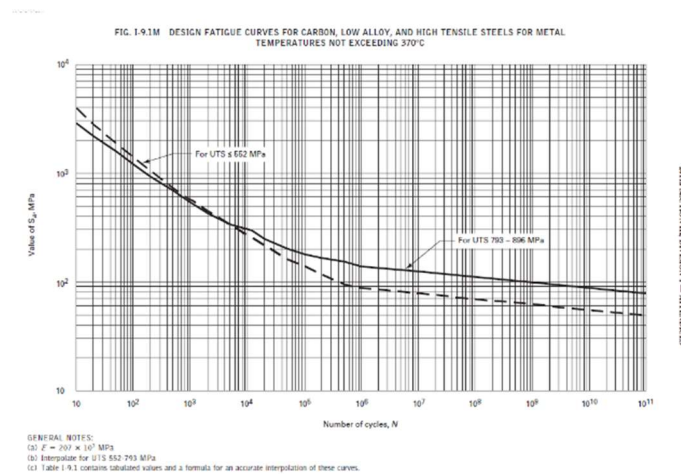
Figure 73: S-N curve

TABLE I-9.1
TABULATED VALUES OF S_a, ksi (MPa), FROM
FIGS. I-9.1 AND I-9.1M

Number of Cycles [Note (1)]	UTS 115-130 ksi (UTS 793-896 MPa)		UTS ≤ 80 ksi (UTS ≤ 552 MPa)	
1E1	420	(2 896)	580	(3 999)
2E1	320	(2 206)	410	(2 827)
5E1	230	(1 586)	275	(1 896)
1E2	175	(1 207)	205	(1 413)
2E2	135	(931)	155	(1 069)
5E2	100	(689)	105	(724)
1E3	78	(538)	83	(572)
2E3	62	(427)	64	(441)
5E3	49	(338)	48	(331)
1E4	44	(303)	38	(262)
1.2E4 [Note (2)]	43	(296)		
2E4	36	(248)	31	(214)
5E4	29	(200)	23	(159)
1E5	26	(179)	20	(138)
2E5	24	(165)	16.5	(114)
5E5	22	(152)	13.5	(93)
1E6	20	(138)	12.5	(86)
1E7	17.8	(123)	11.1	(77)
1E8	15.9	(110)	9.9	(68)
1E9	14.2	(98)	8.8	(61)
1E10	12.6	(87)	7.9	(54)
1E11	11.2	(77)	7.0	(48)

GENERAL NOTES:
(a) All notes in Figs. I-9.1 and I-9.1M apply to this data.
(b) Interpolation between tabular values is permissible based upon data representation by straight lines on log-log plot. See Table I-9.0, General Note (b).

NOTES:
(1) The number of cycles indicated shall be read as follows: *IEJ = I* × 10^J, e.g., 5E6 = 5 × 10^6 or 5,000,000
(2) These data points are included to provide accurate representation of curves at branches or cusps.

Figure 74: Tabular data of the S-N curve

For the cases studied in this thesis, it is of great importance to investigate whether the loading conditions will create fatigue and find the number of cycles that lead to failure. For that to be done, the stress amplitude S_a must be calculated. Based on the data from **Figures 39-42**, the vibrational response has an almost stable maximum value and a minimum value very close to zero. So, an approximate value was calculated $S_a = \sigma_{max}/2$. In **Table 8** the results for Model 1 are displayed for each different case of inlet velocity. Clearly, the only case that fatigue is capable of happening is the last case, for inlet velocity 20 m/s with the critical number of cycles being 10^{11}. It can be calculated that approximately $1.9*10^9\ s$ or 60 years are needed for failure.

Table 8: Stress amplitude for each loading condition of Model 1

u (m/s)	S_a (MPa)
1	8.8
5	11.2
10	18.4
20	46.8

Table 9 lists the same calculations for Model 2. Values for stress amplitude S_a were calculated from the data of **Figures 64-67** in the same way as before. According to the S-N curve none of the loading conditions of Model 2 lead to fatigue as the values are below the endurance limit S_e.

Table 9: Stress amplitude for each loading condition of Model 2

u (m/s)	S_a (MPa)
1	5.05
5	6.4
10	10.6
20	27.15

It is important to clarify that the above fatigue assessment applied only to the curved part of the elbow. The response of the welds was not studied which may become fatigue critical. Moreover, fatigue issues may exist at the pipe supports whose behavior was not examined in this thesis, as well.

5.6. Energy Institute Guidelines

5.6.1. LOF

According to the Energy Institute Guidelines proactive assessments should be carried out on a central pipeline to check for failure. Potential excitation mechanisms should be identified and their risk shall be considered. For each case of external excitation a LOF (likelihood of failure) number should be calculated. This number is calculated for the preventive assessment of an installation and predicts a possible failure. It is not an absolute probability, nor an absolute measure, but a conservative measure for designing purposes. In the specific case where the excitation is caused by Flow Induced Turbulence, the fluid flow produces the turbulent energy and the LOF is given by the following formula

$$LOF = \rho v^2 \, FVF / F_v \qquad (27)$$

where ρ is the density of the fluid, v the velocity of the fluid, FVF is the Fluid Viscosity Factor that takes the value of one for a liquid and F_v is the Flow Induced Vibration factor.

In order to determine F_v, the type of Support Arrangement should be selected. The value of the system's first natural frequency determines the type of piping support and categorizes each system among Stiff, Medium Stiff, Medium, Flexible (according to table T2-1 of the Guidelines). Through this characterization, it is possible to calculate L_{span} and F_v.

L_{span} factor determines how supports will be positioned within the piping system. It expresses the minimum distance between two consecutive supports. It depends only on the stiffness of the system and the outer diameter of the pipes. For a Stiff system it is defined as

$$L_{span} \leq -1.2346 10^{-5} D_{ext}^2 + 0.02 D_{ext} + 2.0563 \qquad (28)$$

F_V factor is the most difficult to determine since it depends on the type of support and the geometric characteristics of the pipes such as the outer diameter and thickness. According to table T2-2 of the Guidelines, for Stiff pipes with an outside diameter of 60 mm - 762 mm the formula for F_V is as follows:

$$F_V = exp[\alpha(D_{ext}/t)^\beta] \qquad (29)$$

where D_{ext} is the external diameter, t is the pipe thickness and α, β:

$$\alpha = 446187 + 6,46 D_{ext} + 9,17*10^{-4} D_{ext}^3 \qquad (30)$$

$$\beta = 0,1 ln(D_{ext}) - 1,3739 \qquad (31)$$

These parameters were calculated for both models and the final results for the LOF number are listed in **Tables 10-11**. Because L_{span} is only dependent on the pipe

diameter it was calculated as L_{span}= 4.87 m for Model 1 and L_{span}= 3.73 m for Model 2.

Table 10: LOF numbers for Model 1

u (m/s)	LOF
1	0.0099
5	0.2466
10	0.9864
20	3.9459

Table 11: LOF numbers for Model 2

u (m/s)	LOF
1	0.0132
5	0.3306
10	1.3225
20	5.29

For a main line piping, Table 3-1 of the Energy Institute Guidelines provides recommendations for the steps to be taken depending on the LOF number. For values of LOF ≥ 1 it is vital that the line is redesigned, reanalyzed and monitored for vibrations. Also, corrective measures shall be taken and the bore connections must be assessed. Finally, a visual inspection has to be undertaken to examine poor construction or support, in addition to possible vibration transmission to other pipe systems. For 0.5 ≤ LOF ≤ 1 the same steps should be followed. However, the situation is not as critical as for the first case. For 0.3 ≤ LOF ≤ 0.5 the effect of small bore connections should be checked alongside a visual survey. For LOF ≤ 0.3 a visual inspection should only be performed. It is clear that for u=10 m/s and u=20 m/s both models are in danger of failure and it is critical for the right measures to be taken.

5.6.2. Vibration Assessment Criteria

A survey method suggested by the Energy Institute about measuring the pipework vibration velocity is analyzed below. In this way, the risk of fatigue induced by vibrations is determined. Velocity is a vector quantity and during vibrational phenomena the absolute value is constantly changing. The RMS velocity is used as a measure of assessing the intensity and direction of the instantaneous velocity. The measured vibration velocity (RMS) alongside the peak frequency of the measured response was considered and based on the diagram of **Figure 75** the size of the problem was evaluated. Three criteria are defined being "Problem", "Concern" and "Acceptable" which indicate fatigue risk. The first two criteria can also be defined by the following formulas

$$Problem\ Vibration: \geq\ 10^{\frac{(\log f+0.48017)}{2.127612}}$$ (32)

$$Concern\ Vibration: \geq\ 10^{\frac{(\log f+1.871083)}{2.084547}}$$ (33)

If the vibration level fits the "Problem" criteria, then control measures should be taken immediately to define the likelihood of failure. If it fits the "Concern" criteria, then there is a possibility for the occurrence of fatigue damage. Control measures should also be taken. For both cases checks on the welds should be performed to ensure fatigue crack has not been initiated.
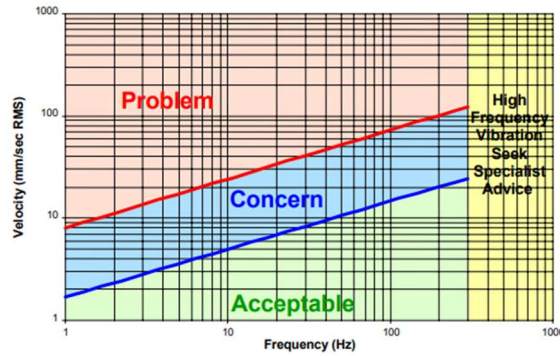
Figure 75: Diagram of Vibration Criteria

Vibration instantaneous velocity represents the rate at which displacement changes. It can be measured as the displacement range over time:

$$u_v = \frac{\Delta s}{\Delta t}$$ (34)

However, the RMS (root mean square) value of velocity must be found from the following formula:

$$RMS = \sqrt{\frac{1}{n}\sum_i x_i^2}$$ (35)

where n is the number of measurements taken and x_i each value. For the specific case studied n expresses the number of velocity measurements and x_i the vibration velocity u_v. Results for each model are listed on **Tables 12-13** following.

Table 12: The velocity measurements for Model 1

u_{inlet} (m/s)	f(Hz)	RMS (mm/s)
1	52	56.4
5	52	70.9
10	52	115.6
20	52	293.6

Table 13: The velocity measurements for Model 2

u_{inlet} (m/s)	f (Hz)	RMS (mm/s)
1	37	44.4
5	37	56.7
10	37	94.2
20	37	239.9

Having the values for the excitation frequency and the RMS velocity the Vibration Criteria were derived. It was concluded that all cases for both models got critical values and were prone to fatigue failure. **Figure 76** depicts the exact points of each loading condition and model on the diagram and shows that they all belong to the "Problem" criteria.

Figure 76: The exact points of concern for the two frequency values

6. CONCLUSIONS

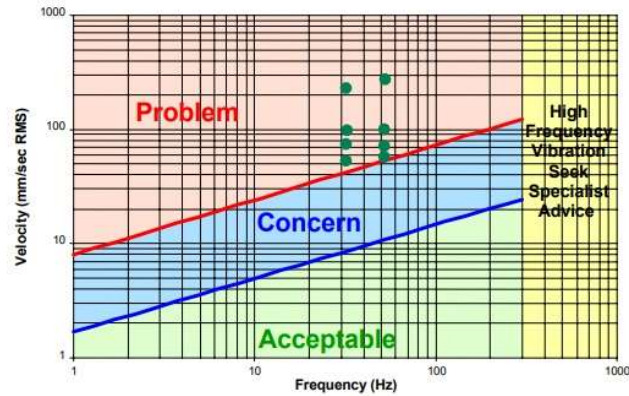Piping systems are mostly used for the transportation of fluids from one place to another. However, when flow disruptions are present such as bends and elbows, significant localized turbulence develops. Turbulence creates a pressure pulsation that leads to the pipe vibrating. This phenomenon is known as Flow Induced Turbulence.

In this thesis, a coupled CFD/FEA analysis was conducted to assess the elbow response when various values of the inlet velocity changed. Two types of pipes were studied with different diameters and radius of curvature. The behavior of the fluid inside the pipes was examined alongside the mechanical response of the pipe. Diagrams for displacement, stress and force produced were displayed. In the end, the possibility of failure of the models due to fatigue was examined.

Regarding the numerical analysis, the fluid exhibited turbulent behavior and the two counterrotating vortexes appeared vividly. The pressure variation was reflected in the fluctuations of the values of the Total Displacement, Equivalent Stress and Force Reaction. The amplitude of the response for all quantities studied increased with the increase of the inlet velocity. At the same time, the oscillations in the passage of time were slightly decreased as a result of the inner damping of the system. This behavior was more intense on Model 1 than Model 2.

Another interesting conclusion was that on Model 1, ovalization of the cross-section was observed, with the maximum stress being on the elbow flank. On the other hand, Model 2 accumulated smaller stresses for the same inlet velocities to Model 1 and exhibited the behavior of a beam under bending. Highest stresses were observed on the bottom fibers that were under compression. This was an effect of the small diameter and the large radius of curvature. Especially, for larger curvatures, the flow's direction is changed more smoothly and, therefore, a decrease appears on the flow vorticity. It should be noted that stresses at the welds connecting the curved part of the elbow with the straight pipe segments were not checked against fatigue in this study. In these areas, stress concentration effects due to the presence of the welds exist, which may become critical for the structural integrity of the elbow. Furthermore, it is anticipated that the vibrations of the pipe will be transferred to the system's supports and their fatigue strength shall be examined as well.

In the end, fatigue strength was tested. For that to be done three methods were employed. Firstly, an S-N curve was used with the help of which it was obtained that fatigue was possible only for Model 1 for the highest inlet velocity studied. For all the other cases, the stress amplitude was lower than the endurance limit. Secondly, according to the Guidelines of the Energy Institute the critical LOF number was calculated. This factor indicated that both models were susceptible to fatigue failure for inlet velocity 10 m/s and 20 m/s. Lastly, by using the diagram of the Vibration Criteria it was demonstrated that for every case studied there was a vibration concern. Hence, it can be suggested that some criteria are more conservative than others and different methods may lead to different results.

Ways to avoid the occurrence of FIV in piping were checked. One way could be, reducing the flow velocity, as it was concluded that the lower the velocity value the lower the amplitude of the response. However, for most applications inlet velocity is a standard property of the system and cannot be changed. It is best to approach the problem from a different perspective by placing an additional support closer to the curved elbow part. By tightening up spaces on supports the system's stiffness increases alongside the natural frequencies, leading to turbulent energy levels falling with frequency. In the numerical simulation conducted it was seen that the presence of the additional supports dissipated all excitation energy and the vibration was completely mitigated.

REFERENCES

[1] Nakamura, Tomomichi, et al., eds. *Flow-induced vibrations: classifications and lessons from practical experiences*. Butterworth-Heinemann, 2013.

[2] Parameshwaran, R., Sai Jathin Dhulipalla, and Daseswara Rao Yendluri. "Fluid-structure interactions and flow induced vibrations: a review." *Procedia Engineering* 144 (2016): 1286-1293.

[3] Grant, Ivan. *Flow induced vibrations in pipes, a finite element approach*. Diss. Cleveland State University, 2010.

[4] Tijsseling, Arris S. "An overview of fluid-structure interaction experiments in single-elbow pipe systems." *Journal of Zhejiang University-SCIENCE A* 20.4 (2019): 233-242.

[5] Kalpakli, Athanasia. *Experimental study of turbulent flows through pipe bends*. Diss. KTH Royal Institute of Technology, 2012.

[6] Zhang, T., Y. O. Zhang, and H. Ouyang. "Structural vibration and fluid-borne noise induced by turbulent flow through a 90 piping elbow with/without a guide vane." *International Journal of Pressure Vessels and Piping* 125 (2015): 66-77.

[7] Chen, Quan, Vimal Vinayan, and Ronald Vrijland. "A Practical Approach to Evaluate Acoustic and Flow Induced Fatigue of Piping Systems." *Offshore Technology Conference*. OnePetro, 2018.

[8] Energy Institute, "Guidelines for the Avoidance of Vibration Induced Fatigue in Process Pipework" 2nd Edition, 2008

[9] Kelly, S. Graham. *Mechanical vibrations: theory and applications*. Cengage learning, 2012.

[10] Tse, Francis Sing, Ivan E. Morse, and Rolland Theodore Hinkle. *Mechanical vibrations*. Boston: Allyn and Bacon, 1963.

[11] Géradin, Michel, and Daniel J. Rixen. *Mechanical vibrations: theory and application to structural dynamics*. John Wiley & Sons, 2014.

[12] Ashby, Michael F., Hugh Shercliff, and David Cebon. Materials: engineering, science, processing and design. Butterworth-Heinemann, 2018.

[13] Gerhart, Philip M., Andrew L. Gerhart, and John I. Hochstein. *Munson, Young and Okiishi's fundamentals of fluid mechanics*. John Wiley & Sons, 2016.

[14] Karamanos, Spyros A. "Mechanical behavior of steel pipe bends: an overview." *Journal of Pressure Vessel Technology* 138.4 (2016).

[15] Spedding, P. L., Emmanuel Bénard, and G. M. McNally. "Fluid flow through 90 degree bends." *Developments in Chemical Engineering and Mineral Processing* 12.1-2 (2004): 107-128.

[16] Kim, Jongtae, Mohan Yadav, and Seungjin Kim. "Characteristics of secondary flow induced by 90-degree elbow in turbulent pipe flow." *Engineering Applications of Computational Fluid Mechanics* 8.2 (2014): 229-239.

[17] Dean, Wo R. "XVI. Note on the motion of fluid in a curved pipe." *The London, Edinburgh, and Dublin Philosophical Magazine and Journal of Science* 4.20 (1927): 208-223.

[18] Ito, H. "Pressure losses in smooth pipe bends." (1960): 131-140.

[19] Hawthorne, William Rede. "Secondary circulation in fluid flow." *Proceedings of the Royal Society of London. Series A. Mathematical and Physical Sciences* 206.1086 (1951): 374-387.

[20] Kim, Jongtae, Mohan Yadav, and Seungjin Kim. "Characteristics of secondary flow induced by 90-degree elbow in turbulent pipe flow." *Engineering Applications of Computational Fluid Mechanics* 8.2 (2014): 229-239.

[21] Kaldy, Z., and O. Ayala. "Quantitative Assessment of Secondary Flows of Single-phase Fluid through Pipe Bends." (2016).

[22] Crawford, N., et al. "A numerical investigation of the flow structures and losses for turbulent flow in 90 elbow bends." *Proceedings of the Institution of Mechanical Engineers, Part E: Journal of Process Mechanical Engineering* 223.1 (2009): 27-44.

[23] Von Karman, T. "Uber die formuanderung dunnwandiger rohre [in German." *Zeit. Des Vereines Deutcher Ingenieure* 55 (1911): 1889-1895.

[24] Rodabaugh, ECf, and H. H. George. "Effect of internal pressure on flexibility and stress-intensification factors of curved pipe or welding elbows." *Transactions of the American Society of Mechanical Engineers* 79.4 (1957): 939-948.

[25] Edmunds, H. G., and F. J. Beer. "Notes on incremental collapse in pressure vessels." *Journal of Mechanical Engineering Science* 3.3 (1961): 187-199.

[26] Moreton, D. N., K. Yahiaoui, and D. G. Moffat. "Onset of ratchetting in pressurised piping elbows subjected to in-plane bending moments." *International journal of pressure vessels and piping* 68.1 (1996): 73-79.

[27] Yahiaoui, K., D. G. Moffat, and D. N. Moreton. "Response and cyclic strain accumulation of pressurized piping elbows under dynamic in-plane bending." *The Journal of Strain Analysis for Engineering Design* 31.2 (1996): 135-151.

[28] DeGrassi, G., et al. "BNL Nonlinear Pre-Test Seismic Analysis for the NUPEC Ultimate Strength Piping Test Program (K255)." (2003).

[29] Karamanos, S., et al. "Structural safety of industrial steel tanks, pressure vessels and piping systems under seismic loading." *INDUSE Project, Research Fund for Coal and Steel, European Union, Luxembourg, Final Report No. RFSR-CT-2009-00022* (2013).

[30] Varelis, George E., Patricia Pappa, and Spyros A. Karamanos. "Finite element analysis of industrial steel elbows under strong cyclic loading." *Pressure Vessels and Piping Conference*. Vol. 44588. 2011.

[31] Varelis, George E., Spyros A. Karamanos, and A. M. Gresnigt. "Steel elbow response under strong cyclic loading." *The Twenty-second International Offshore and Polar Engineering Conference*. OnePetro, 2012.

[32] Varelis, George E., and Spyros A. Karamanos. "Low-cycle fatigue of pressurized steel elbows under in-plane bending." *Journal of Pressure Vessel Technology* 137.1 (2015).

[33] Wiggert, David C., and Arris S. Tijsseling. "Fluid transients and fluid-structure interaction in flexible liquid-filled piping." *Appl. Mech. Rev.* 54.5 (2001): 455-481.

[34] Ferras, David, et al. "One-dimensional fluid–structure interaction models in pressurized fluid-filled pipes: A review." *Applied Sciences* 8.10 (2018): 1844.